Politechnika Wrocławska

**FIELD OF SCIENCE: ELECTRICAL ENGINEERING**

DISCIPLINE OF SCIENCE: AUTOMATION, ELECTRONICS, ELECTRICAL ENGINEERING AND SPACE TECHNOLOGIES

# DOCTORAL DISSERTATION

## Enhancing operational capability of Islanded Microgrids through Optimal Multiple Droop-based DG Placements

Tham Xuan Nguyen

Supervisor:
Dr hab. inż. Robert Lis, Prof. uczelni

Keywords: Islanded microgrid, lost power mitigation, voltage stability, dispatchable distributed generator, droop law, optimal sizing and siting, multiple droop-DG sites, modified backward-forward sweep load flow, honey badger technique, differential evolution technique.

WROCŁAW 2024

# ACKNOWLEDGEMENT

I would like to deeply thank my beloved family, Lao Huynh, Thieu Nguyen, Phuong Nguyen, Thuat Nguyen, Thuoc Nguyen, Le Dang, and Toan Nguyen, for their endless love, unconditional support, and encouragement in my pursuit of dream.

I profoundly thank my supervisor, Prof. Robert Lis for his invaluable advice, continuous support, and patience. His vast experience and wealth of knowledge have inspired me both in daily life and in the academy.

My deep appreciation goes to Vietnam and Poland governments for financial support with the NAWA scholarship during my Ph.D. study.

My gratitude extends to the Rector of Quy Nhon University, the Dean, and my colleagues at the Department of Electrical Engineering, the Faculty of Engineering and Technology for their support in facilitating my Ph.D. study in Poland.

The author expresses sincere thanks to Prof. Piotr Chrzan at Gdańsk University of Technology and Dr. Ho Le at Quy Nhon University for their invaluable assistance in writing a letter of recommendation for my scholarship in Poland.

The sincere thanks are extended to Mr. Mateusz Jędrzejewski and Ms. Agnieszka Pławecka at Wrocław University of Science and Technology for their technical assistance in my research on supercomputer systems, particularly BEM2 and PLANTON-U3.

My deep gratitude extends to my friends, Dr. Co Nguyen and Mr. Hung Nguyen, for their support in improving my academic writing skills.

To my parents, Thieu Van Nguyen and Phuong Thi Nguyen.

# ABSTRACT

Islanded microgrids, defined by their self-healing characteristics, are a crucial part of a state-of-the-art grid and support the vision of a resilient and sustainable infrastructure of the future.

Droop-based distributed and dispersed generators (DG) within microgrid off-grid operation mention DGs in a microgrid that use a control algorithm determined by the properties of frequency and voltage droop gains. These techniques allow DGs to regulate their production power in response to variations in voltage and frequency.

Robust methodologies are described by their systematic and resilient nature, aiming to yield stability, adaptability, and dependability in the face of shifting barriers and uncertainties. It is necessary to reach accurate and dependable findings in the analysis of electrical systems.

The Modified Backward-Forward Sweep (MBFS) load flow approach is a numerical method employed to determine the energy flow in the power grid and identify optimal operational points. The backward-forward sweep is a computational technique that verifies that the power flow equations, together with operational constraints, are met at each bus by starting at the termination of the electric power system (load nodes), moving backward to the source (generator nodes), and then forward again. The 'modified' in MBFS, an expansion of the conventional backward-forward sweep technique, aims to enhance the accuracy and speed of its convergence.

Distributed and dispersed generator with compact size is preferred for deployment in microgrid networks (MG), including both grid-on and islanded modes, due to economic and technical benefits. Operating in the islanded microgrid mode,

the DGs within the system control the microgrid voltage frequency and magnitude inside the intended bounds. In this operational scenario, DGs frequently use the droop law to share power for load due to their advantages, including the low cost of control and communication systems, inherent flexibility, and expandability. Employing droop-based DGs in microgrid grid-off operations significantly advances the future grid.

The operation of DGs through the droop law in off-grid MGs offers many benefits, as mentioned above. However, variations in local load over time, along with inappropriate output power of droop-DGs throughout the operational process, impact power quality and regulate system voltage and efficient energy use. For these issues, this thesis focusses on addressing the optimal planning of droop-DGs in an islanded MG, namely suitable droop parameters (size) and placement using robust methodologies such as the MBFS power flow approach, and Differential Evolution and Honey Badger techniques-based metaheuristic algorithms. The primary objective is to diminish lost power and gain bus voltage.

The number and positioning of DGs affect the extent of mitigation of lost power in distribution networks. Therefore, this thesis also investigates the effect of installing the appropriate multiple-droop-DG locations within an islanded MG, taking into account time-varying load, to maximise potential lost power minimisation and increase the islanded MG voltage profile. To this end, the proposed methodologies consisting of the MBFS load flow approach and the Differential Evolution technique are used to tackle the problem mentioned above.

The simulation results achieved provide evidence of the productivity and superiority of the suggested techniques in contrast to pre-existing works for the proposed problems.

# CONTENTS

# LIST OF FIGURES

# LIST OF TABLES

# ABBREVIATIONS

| | |
|---|---|
| AC | Alternating Current |
| AMG | Autonomous Microgrid |
| BCBV | Branch Current to Bus Voltage |
| BESD | Battery Electric Storage Device |
| BIBC | Bus-Injection to Branch-Current |
| CB | Capacitor Bank |
| CSI-IP | Combined Sensitivity Index-Iterative Procedure |
| CSI-PSO | Combined Sensitivity Index-Particle Swarm Optimisation |
| DDG | Droop Distributed Generator |
| DE | Differential Evolution |
| DG | Distributed Generator |
| DIMG | Droop-based Islanded Microgrid |
| DL | Dump Load |
| DN | Distribution Network |
| DR | Distributed Resource |
| DSM | Demand Side Management |
| DSTATCOM | Distribution Static Compensator |
| ED | Economic Dispatch |
| EBD | Energy Backup Device |
| EV | Electric Vehicle |
| GA | Genetic Algorithm |
| GWO | Grey Wolf Optimiser |
| HB | Honey Badger |
| HS | Harmony Search |
| IMG | Islanded Microgrid |

| | |
|---|---|
| MBFS | Modified Backward-Forward Sweep |
| MG | Microgrid |
| MILP | Mixed-Integer Linear Programming |
| MINLP | Mixed Integer Nonlinear Programming |
| MOPSO | Multi-Objective Particle Swarm Optimisation |
| MT | Microturbine |
| NDIMG | Non-Droop-based Islanded Microgrid |
| NLTV-MOPSO | Non-Linear Time-Varying Multi-Objective Particle Swarm Optimisation |
| NSGA | Non-Dominated Sorted Genetic Algorithm |
| PID | Proportional Integral Derivative |
| PSO | Particle Swarm Optimisation |
| PV | Photovoltaic |
| RS | Renewable Source |
| RG | Renewable Generation |
| SC | Shunt Capacitor |
| SF | Switchable and Fixed |
| SR | Sensitivity Region |
| STATCOM | Static Synchronous Compensator |
| TV-MOPSO | Time-Varying Multi-Objective Particle Swarm Optimisation |
| UC | Unit Commitment |
| VAR | Volt-Ampere Reactive |
| VB | Virtual Bus |
| VSI | Voltage Stability Index |
| VVC | Volt-Var Control |
| WT | Wind Turbine |

# CHAPTER

# 1

# INTRODUCTION

## 1.1 Research Motivation

Based on statistical data from [1], it is estimated that approximately 670 million people worldwide will not be able to access electricity in 2030. The majority of these individuals reside in remote places, such as isolated regions, outlying areas, and remote islands, where linking to the national electric system is challenging. For this reason, electrification of places without power is essential for the advancement of society and the economy. To address this issue, state-of-the-art technologies, such as compact distributed generators (DG), have been developed, which can be installed easily and flexibly in the previously mentioned areas.

Microgrid (MG) is a modern electric system that encompasses renewable and non-renewable resource-based DGs, distributed energy backup devices (EBD), and consumer loads operating at distribution voltage levels [2]. The on-grid (i.e., grid-connected) and off-grid (i.e., islanded MG) modes are both supported for operation. The national grid is in charge of adjusting the system voltage frequency and magnitude inside a predetermined bound when the system is in the on-grid MG mode. During islanded microgrid (IMG) mode, each grid DG is responsible for adjusting the IMG voltage's frequency and magnitude inside predefined bounds if a slack bus does not exist.

Within an off-grid microgrid mode, the frequency and magnitude regulation of the MG voltage is managed by the DGs comprising the grid. In this context, DGs frequently utilise droop-based operations due to their ability to reduce the cost of control and communication systems, improve dependable system, and their inherent flexibility and expandability. Furthermore, as detailed in IEEE Std 1547™-2018 [3], DGs functioning in off-grid microgrids offer a wide range of benefits compared to their on-grid microgrids. These benefits include minimising lost power, improving power quality, providing a dependable source of supply, simple local power grid expansion, etc. The use of DGs in the autonomous operation of IMGs contributes considerably to the construction and advancement of the future grid [3], [4].

However, the planning and management of droop-based islanded microgrids (DIMG) face several significant challenges. These challenges include dealing with the uncertainty of local load fluctuations, ensuring effective power sharing among droop-DGs, and determining optimal DG placement and size.

This thesis focusses primarily on solving the following two problems. Firstly, in the face of load fluctuations, it is imperative in order to keep islanded microgrid voltage frequency and magnitude inside predefined standards. As a result, selecting the appropriate droop parameters and positioning for the DGs are crucial to lowering lost power and gaining nodal voltage stability margin and voltage. Secondly, the optimal deployment of multiple DG positions in a DIMG through the droop operation is regarded as a means to mitigate line losses and improve nodal voltages. This not only leads to fuel savings, but also reduces overall operational and maintenance costs. This thesis aims to build a proper mathematical model and an efficient algorithm capable of addressing the challenges mentioned above effectively.

## 1.2 Methodologies for the optimal allocation of droop-DGs in an IMG

There is no universally suitable algorithm for all optimisation problems, as indicated in Ref. [5]. Consequently, the task of selecting/developing an efficient algorithm to address the proposed research proves to be a challenge. In this thesis, the capabilities of two distinct metaheuristic algorithms, differential evolution (DE) and honey badger (HB), are exploited, with an emphasis on the prominent role played by the modified backward-forward sweep (MBFS) load flow approach. The integration of these methodologies forms a strategic approach employed to optimise the location and capacity of droop-DGs within the IMG's planning framework.

### 1.2.1 Differential Evolution technique

The DE technique, first presented in 1995 by the researchers Price and Storn [6], is an inhabitants-based optimisation technique widely applicable in various domains of problems, including engineering design, computational fluid dynamics, and electrical power systems, among others [7].

The DE technique has been introduced for identifying the management, location, and allocation of non-renewable and renewable generators within distribution networks (DN), with a primary focus on maximising power loss reduction and increasing the penetration capacity of renewable DGs [8]. The researchers in [9] presented the use of various mutation strategies of the DE algorithm to optimise reactive power planning for existing volt-ampere reactive power sources (VAR), such as generators and transformers, within Egyptian DN. The primary aim was to minimise the lost energy and investment costs of the device. In Ref. [10], the authors proposed the DE technique for the optimal microgrid energy management system, encompassing fuel cells (FC), renewable generations of solar photovoltaic (PV) plants and wind turbines (WT), with the overarching goal of minimising fuel expenses. Reference [11] introduced a hybrid approach combining DE technique, Strength Pareto Evolutionary technique, and genetic algorithm (GA) to find the positioning of solar and wind renewable generators and capacitor bank (CB) systems within the grid, while considering uncertainties related to renewable sources (RS), load variations, and demand for electric vehicles (EV). This approach was designed to improve the voltage stability index (VSI), reduce $CO_2$ emissions, and minimise installation, operation, and maintenance costs. In Ref. [12], a modified DE technique version, mentioned as self-balanced DE, is developed to optimise the reactive power dispatch of generators, transformers, and CBs, with the goal of minimising lost active power.

### 1.2.2 Honey Badger technique

The HB technique first presented by Hashim et al. in 2022 [13], emerged as an effective optimisation method for use in practical applications such as predicting COVID-19 [14], effective load balancing for wireless 5G [15], skin cancer detection [16], optimal size of standalone RS systems [17], etc.

The HB algorithm has also been applied to address operational and planning challenges within the electrical power system, as evidenced in references [18], [19], [20], [21], [22]. In [18], the HB approach has been utilised to adjust the parameters of the proportional integral derivative (PID) setup, with the objective of minimising voltage and frequency deviations within an IMG, particularly during sudden changes or load disturbances, and in the absence of a robust control system. Reference [19] saw the development of a mathematical model to optimise energy use in on-grid microgrid that incorporates renewable DG, microturbine (MT), battery electric storage device (BESD), and fuel cell using the HB algorithm. The goal was to simultaneously minimise operating costs and environmental pollutant emissions. Kamarzaman et al. [20] developed the HB technique to identify the ideal size of PV modules within a standalone grid that integrates a diesel generator and BESD, with the aim of enhancing the reliable source supply. In [21], the HB algorithm has been utilised to dispatch reactive power from transformers and CBs to mitigate transmission line losses and bus voltage deviations in IEEE 30-bus DN. To address the problem of system frequency stability under load changes and stochastic intermittency of RS, Khadanga et al. [22] developed the HB algorithm to regularise the settings of fractional-order PID controllers.

### 1.2.3 MBFS load flow approach

The MBFS technique, initially presented in 2017 by Hameed et al. [23], holds a crucial role in identifying the optimal operational point of DIMG networks. Remarkably, its versatility extends to computing load flow within radial and ill-conditioned autonomous microgrids (AMG) [24]. This efficiency is attributed to its dependence on linear equations, which eliminates the need for variable derivatives and the Hessian matrix [25].

The MBFS method serves to compute the proper placement and capacity of dump loads (DL) within IMGs and weakly meshed grids [26], [27], [28], with the primary objective of mitigating voltage deviation and frequency deviation. In [26], an analytical method is developed to optimise the placement of DLs in AMG, focussing on reducing power mismatches during peak hours of RS and low load conditions under high penetration of RS. Ref. [27] introduced the modified whale optimisation algorithm and the non-dominated sorted genetic algorithm-II (NSGA-II) for DL siting within weakly meshed grids operating within the autonomous mode of the microgrid. Furthermore, in [28], an improved MBFS approach coupled with a mixed integer distributed ant colony algorithm minimises power losses in IMG between times of low load demand and high RS generation. Reference [29] presented robust optimisation techniques, Sensitivity Region (SR) and Feasibility-SR, to assess the hosting capacity of RS in an IMG, taking into account the stochasticity of RS and the variation in load, while the MBFS approach is utilised to meet operational criteria. Ashfaq et al. [30] introduced a novel load flow approach-based MBFS technique to optimise DG placement in regionalised IMG, distinguishing between droop and renewable regions based on DG, with the goal of improving the speed of problem convergence.

## 1.3 Droop control method

Within IMG grids, the droop technique is applied to control dispatchable DGs, with the aim of sharing load power among these DGs. This technique allows dispatchable DGs to connect in parallel. The concept of the droop control originated from the behaviour seen in traditional synchronous generators, in which the frequency decreases as the load demand for power increases, as presented in [31]. The IMG voltage magnitude and frequency can be adjusted through the droop parameters (i.e., $m_p, n_q,$ and $|V_{ref}|$) from droop-based generators.

The benefit of the droop technique is the reduction in the cost of communication systems, the improvement of a reliable system, and the flexibility and expandability. However, the droop operation has some disadvantages: poor harmonic sharing caused by nonlinear loads and power mismatch on the line impedance between parallel inverters.

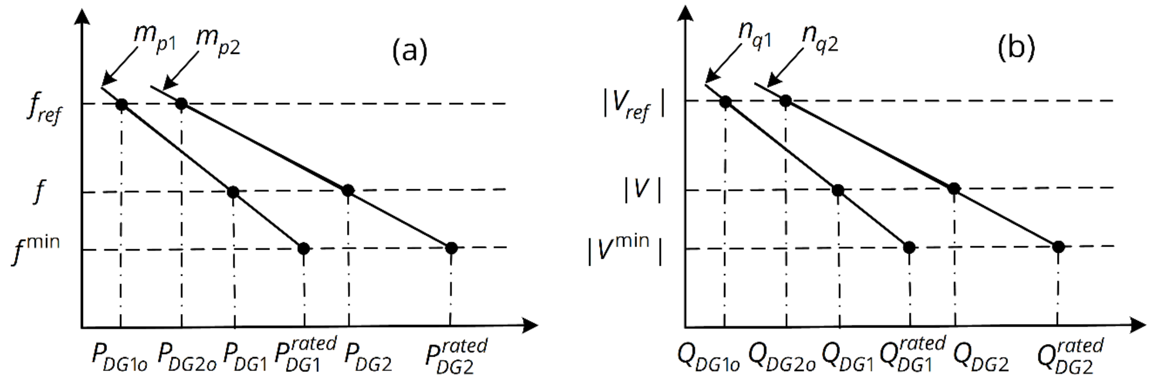


Fig. 1. 1 Droop properties: (a) $P-f$ droop laws; (b) $Q-V$ droop laws

Within droop-DG-based IMGs, active power sharing is tuned through the real power droop gain $m_p$, as depicted in Fig. 1. 1(a). The droop equation related to active power sharing can be described in [23]

$$f = f_{ref} + m_{pi}(P_{DGi} - P_{DGio}) \tag{1.1}$$

where: $f_{ref}$ and $f$ represent the reference and working frequency; $P_{DGi}$ denotes the production power of the droop-DG at node $i$, $\forall i \in \{1, 2, ..., N\}$, $N$ signifies the number of nodes within the grid; the droop-DG's power reference point at node $i$ is expressed as $P_{DGio}$; $m_{pi}$ denotes the droop gain of the DG frequency.

Each dispatchable droop-DG operates in the islanded MG mode, and it is first created to supply the output of active power $P_{DGio}$ according to the reference frequency $f_{ref}$, as illustrated in Fig. 1. 1(a) [32]. When the frequency of IMG fluctuates due to the current generation and consumer power mismatch, DGs should regulate their power outputs at a permissible level through their droop gains $m_{pi}$ to power all loads on the grid at the steady-state frequency of $f$. This approach enables the predetermined sharing of total load demands between droop-DGs based on their individual rated active powers.

Reactive power sharing in the IMG grid is adjusted by reactive power droop gain $n_q$ and reference voltage magnitude $|V_{ref}|$, as depicted in Fig. 1. 1(b). This approach can be mathematically modelled by [23]

$$|V_i| = |V_{refi}| + n_{qi}(Q_{DGi} - Q_{DGio}) \tag{1.2}$$

where: $Q_{DGi}$ denotes the production power of the droop-DG at node $i$, the droop-DG's power reference point at node $i$ is denoted as $Q_{DGio}$, and $n_{qi}$ signifies the $V$ droop coefficient, while $|V_i|$ and $|V_{refi}|$ are its terminal and reference voltage magnitudes.

Similar to $P-f$ characteristics, in islanded MG mode of functioning, each droop-DG is first created to provide the output of reactive power $Q_{DGio}$ at the reference voltage magnitude $|V_{refi}|$, as depicted in Fig. 1. 1(b). By tuning droop gain $n_{qi}$ and reference voltage $|V_{refi}|$ inside respective limits, DGs can control their reactive power outputs at a permitted level, allowing them to satisfy load requirements at the operating voltage magnitude of $|V_i|$ when the droop-DG's terminal voltage changes resulting from the reactive power mismatch during the operational process. By using this approach, the load demands of the droop-DGs can be pre-shared according to their respective rated reactive powers.

The accuracy of power sharing in the grid depends on the option of the proper droop equations of the DG for each investigated power grid, as expressed in Subsection 3.3.2 of Chapter 3. The mathematical model for tuning DG droop parameters within predefined ranges is described in more detail in Subsection 3.3.4 of Chapter 3.

## 1.4 Research Problem Statement

Research problems are addressed in this thesis and are outlined below.

- To begin with, the selection of the appropriate power flow approach for computing an IMG's working point is crucial. The significance of this study is also twofold: It relates to the formulation of a proper mathematical model and the development of an efficient algorithm. These considerations are used to identify the droop parameters of DGs, including their $P$ and $Q$ droop gains and reference voltage magnitudes. The ultimate aim is to tune these parameters to the corresponding sites of the DGs to ensure that they can effectively meet a load that changes over time while simultaneously minimising lost power and enhancing bus voltage.

- Second, the extent of mitigating lost power in IMGs is dependent upon the number of DG placements [33]. Therefore, the investigation of optimising the sites of multiple droop-DGs is a significant research objective. In this thesis, the development of a proper model of mathematics and an effective algorithm to tackle the problem mentioned is also considered.

## 1.5 Contributions of Research

Optimal planning, including the capacity and positioning of droop-DGs in an IMG, is essential. It significantly contributes to efficient energy use, improved power quality, easy operation and maintenance, and the development of the future power grid infrastructure. This thesis focusses on the establishment of a mathematical model to find the rating and placement of droop-DGs within the off-grid microgrid considering uncertainty of local load and various constraint conditions. Additionally, efficient metaheuristic algorithms are also developed to find the appropriate droop parameters for DGs at their respective sites in an islanded microgrid. Furthermore, the problem of optimising the number of DG sites within an islanded microgrid is also concerned, with the purpose of maximising the minimisation of power losses.

The primary task of this thesis is to show that the lost active and reactive power within the DIMG grid is considerably mitigated, and nodal voltage magnitudes are also improved through robust methodologies for both the proper allocation (i.e., capacity and positioning) of droop-DGs and the optimal deployment of multiple droop-DG placements within the DIMG grid. The outcomes achieved demonstrate that the extent of lost power mitigation and bus voltage level are the best when installing suitable multiple droop-DG units on the grid. This thesis statement is proven in the following main contributions:

1. The selection of the appropriate load flow method for a DIMG is significant for identifying optimal operational points and a lower computational burden; In this thesis, the robust MBFS load flow approach is applied to resolve both the proper position and sizing of the droop-DGs within the IMG and multiple droop-DG sites in the IMG grid, taking into account local load uncertainty.

2. Robust and reliable Differential Evolution and Honey Badger techniques, focused on optimising droop parameters and DG placement in an islanded microgrid, excel in effectively adapting to the variations in time-varying local load demands, aims to mitigate lost power, and boost bus voltage.

3. Deploying multiple DG placements with the purpose of maximising lost power mitigation and simultaneously improving nodal voltage using droop operation in an IMG, using the powerful DE technique.

## 1.6 The scope of thesis

This thesis focusses primarily on optimising the allocation of droop-DGs and deploying multiple droop-DG units within an islanded mode of radial microgrid networks. Furthermore, on the examined power grid, a maximum of five droop-DGs are installed to fulfil the load. The aim of these tasks is to lower lost power and gain IMG power quality throughout operational processes.

## 1.7 Structure of thesis

In Chapter 1, the motivation for the implementation of this thesis is presented, along with the research problem. Then a survey of several studies related to the proposed methodologies that are used for the identification of the proper size and site of droop-DGs in IMGs, specifically the DE and HB techniques and the MBFS method. The description of droop control method, research problem statement, contributions, scope of research, and structure of thesis can be found at the end of this chapter.

Chapter 2 gives a comprehensive review of existing studies concerning both the appropriate allocation of DG in a DIMG and the impact analysis of deploying multiple droop-DG sites in a DIMG to minimise line loss and improve bus voltage.

In Chapter 3, the suggested methodologies to tackle the proper allocation, including size and site of droop-DGs within an IMG are described in more detail consisting of the DE and HB techniques, the MBFS load flow approach, and a mathematical model formulation to optimise the DG droop parameters. Specifically, the linear equation-based MBFS approach is employed to identify the ideal operating points of the IMG using the droop strategy.

Chapter 4 expresses a mathematical modelling for droop-DGs size and site in an IEEE 33-bus IMG incorporating various operational constraints. The DE and HB techniques are then developed to determine the proper droop parameters of the DGs for their respective sites. Additionally, the MBFS technique is used to compute the energy flow in branches of the grid corresponding to different load profiles. The results achieved after the simulation demonstrate that the HB algorithm outperforms the DE technique in mitigating lost power and increasing nodal voltage when resolving the proper allocation of droop-DGs within the DIMG.

In Chapter 5, the impact of deploying multiple droop-DG placements in a DIMG to maximise lost power minimisation and enhance voltage profile is investigated and analysed, considering the variation of load demand. In this chapter, the DE algorithm is utilised to find appropriate multiple droop-DG locations on the grid, while the MBFS approach is to determine the energy flow in the DIMG and satisfy operational constraints. The efficacy of the DE technique for the selected cases is contrasted with some previous techniques. The simulation outcomes obtained demonstrate that the suggested DE technique works well to detect the best multiple droop-DG sites.

Chapter 6 comprises conclusions and ideas for further research.

# CHAPTER

# 2

# LITERATURE REVIEW

## 2.1 Related work of planning (placement and size) of Droop-DG for Islanded AC Microgrid

Two main categories can be employed to ascertain where distributed resources (DR) should be placed within IMG networks. The first category resolves the question of DR capacity, while the second is about optimising their allocation and location at the same time.

The determination of the appropriate size for DRs can be achieved through a variety of well-established techniques within both non-droop-based IMG (NDIMG) [34], [35], [36], [37], [38], [39], [40], [41], [42] and DIMG [29], [43], [44], [45], [46], [47], [48], [49], [50], [51]. The details of each approach are presented as follows:

- The optimal BESD size is addressed to effectively mitigate the power fluctuations originating from wind and solar-based DRs, and the local and EV loads [34]. In Ref. [35] proposed using GridLab-D tool to optimise BESD capacity in an IMG for minimising the total cost. Lee et al. [36] applied a pattern search algorithm to find the appropriate reserve capacity in an IMG to control the operating frequency. Reference [37] introduced a particle swarm optimisation algorithm (PSO) for BESD size with the aim of adjusting the frequency of the standalone microgrid and minimising the overall cost of BESD, considering the presence of a solar PV plant. Furthermore, Ref. [38] presented an integrated algorithm designed to optimise the size of a hydrogen-based EBD, with the aim of enhancing the penetration level of RS within an autonomous network. In [39], optimal energy management is proposed in an NDIMG using the General Algebraic Modelling System tool considering the capacity and number of renewable generations (RG) to minimise operational and reactive power costs. Reference [40], a bi-objective model used to optimise RG and EBD sizes in standalone microgrids that account for the supply risk and cost. The use of a distributionally robust strategy with the Wasserstein metric deals with load supply risk. In [41], the HOME tool is proposed for the ideal capacity of island areas within Taiwan considering techno-economic issues. The authors in [42] proposed a discrete Fourier transform technique for rating of diesel generators and EBD within an IMG. The optimal values of the cut-off frequency balance the costs of capital and fuel for economic size.

- Zang et al. presented a hybrid approach that combines the GA toolbox, the sensitivity region method, and feasibility-SR is introduced to find the hosting capacity of RS within a DIMG [29]. Ref. [43] employed a weighted aggregate sum-based grey wolf optimiser (GWO) for the suitable size of droop distributed generator (DDG), renewable DG, and BESD within a DIMG, with the primary goal of minimising operating and maintenance costs, loss of lines, and emissions. Roy et al. [44] focused on optimising the size of DDGs, RGs, and CBs within a DIMG network, employing a hybrid methodology known as multi-objective PSO (MOPSO) and fuzzy to achieve reductions in lost active power, operation cost, and $CO_2$ emissions. In [45], the optimal EBD size is to adjust the primary frequency of self-sustainable DIMGs within predefined limits, addressing the inherent stochastic nature of intermittent RSs. Reference [46], solar PV plant and BESD-based DIMG size are calculated by adjusting DG's droop parameters to minimise fuel price, emissions and variations in voltage. The optimal droop parameters of DG are developed in a DIMG with RG [47] and an integrated battery [48]. In [47], a fuzzy approach and a PSO algorithm are used for the size of the microgrid. Hong's point estimate models the variation of electric load and RG. The aim of the study in

[48] was to minimise cost and emission and meet the heat demand. BESD capacity is conducted on a DIMG [49] and a standalone microgrid [50]. Ref. [49] used BESD to adjust the primary frequency, considering the properties of short-term overload of BESD. In [50], the fluctuation in the microgrid working frequency is significantly decreased due to the presence of BESD. This deviation arises from the increasing level of penetration of renewable DGs. In [51], the optimal size of a DIMG considers the cost and dependability of the electricity supply; however, the MG's power losses is disregarded.

Various techniques have been developed to tune the setting of the DG droop parameters in IMGs throughout the operation processes for the following purposes:

- Adjusting the operating frequency and voltage of IMG using bifurcation theory [52], multiplayer optimisation [53], probabilistic analytical technique [54] and PSO [55].
- Minimising lost active powers and voltage deviations using the artificial bee colony technique [56].
- Improving reactive power sharing for grid voltage regulation [57], [58] with an analytical method as in Ref. [58].

To solve technical issues consisting of overvoltage and reverse load flow [59], [60] induced by the high integration of RGs into microgrids, and increase the injected power into the grid from renewable DG, devices such as BESD, static synchronous compensator (STATCOM), distribution static compensator (DSTATCOM) and PV-STATCOM are often suggested. In renewable sources-based primarily microgrids, BESD is prioritised for the above-mentioned goals due to its flexibility in periods when the generation of RS is high and the load is low, especially in peak shaving applications [61], [62], [63], [64]. Resolving the proper size of BESD through economic dispatch (ED) while factoring in power losses and satisfying operational constraints within an islanded MG emerges as a multifaceted challenge that includes studies of both DGs without using droop operation [65], [66], [67], [68], [69], [70], [71], [72], [73] and within droop control [74].

- Salman et al. examined the capacity of BESD, considering the variation of DG driven by wind turbine and load demands [65]. The impacts of a dump load on the optimised model are also considered. Kirthiga et al. [66] developed a hybrid GA and PSO methodology for the ideal sizing of MTs, solar and wind plants, and BESDs to minimise generator installation costs, mitigate losses, and improve nodal voltage. Reference [67], the cost minimisation for the RS and EBD unit commitment schedules (UC) is solved using a mixed linear integer approach. A forward neural network-based machine learning is proposed to forecast RS output power and mitigate losses. In [68], a novel UC problem is introduced to identify the appropriate size of battery bank systems in conjunction with WTs. This approach, known as the Here-and-Now method, aims to reduce the total cost. Reference [69] developed mixed integer nonlinear programming (MINLP) to resolve the UC issue while incorporating demand response approach (DR), considering various operational constraints. The objective was to optimise the BESD capacity and simultaneously meet operational constraints. Sufyan et al. [70] used a firefly algorithm in order to optimise economical planning with battery capacity in RG-based IMG considering the lifespan of BESD. The PSO approach has been introduced in [71] to identify the proper location of hydrogen-based energy storage capacity in IMG integrating renewable DG. In [72], the MINLP model is resolved through a two-stage decomposition approach. The first involved determining the proper BESD ratings, and the second calculated the optimal installation year. Ref. [73] developed a novel convex technique for the BESD rating within an IMG to reduce the entire price.
- Hesaroor et al. investigated the optimal BESD size within DIMGs, with a focus on integration of the ED problem [74]. A new heuristic programme is developed for the optimal charge and discharge strategies of BESD.

The ideal size of the off-grid network determined by the demand side management strategy (DSM) [75], demand response [76], [77], [78], [79].

- Khezri et al. presented a new DSM method using the fuzzy logic for the proper size of solar PV, WT, and BESD integration for the whole house considering the degradation of battery capacity [75].
- The PSO technique is developed for the proper capacity of a standalone grid while taking into account incentive-based DR [76]. In WT, solar PV plant-based off-grid microgrid, as mentioned in [77], the best capacity for different types of battery system is obtained through the incentive-based DR approach and the exchange market algorithm. The researchers in [78] introduced a mixed-integer linear programming technique (MILP) in order to optimise the size and operational schedule of an IMG considering the DR approach. The aim was to minimise the mismatch between generation capacity and consumer load, as well as the total cost. In [79], the load-shifting approach is introduced to meet air conditioning and heating ventilation loads. An autoregressive moving average model has been used for the stochastic analysis of solar and wind resource-based generators and load.

Previous studies introduced several methodologies for the ideal DG size and placement within NDIMG [33], [80], [81], [82], [83], [84], [85], [86], [87], [88], [89], [90]. Positioning DG units without considering the droop strategy involves the transformation of standard DN to create islanded topology [80], [81], [83], [86], [87]. In [80], effective load flow and active power injection approaches are used to find the suitable DG location. Subsequently, the proper DG size is achieved through the PSO technique. Reference [81] evaluated the effects of placing multiple DGs to minimise energy losses. Kayalvizhi et al. [83] developed a harmony search technique (HS) for the operation and planning of an autonomous MG integrated DR to lower lost energy, voltage deviation, and the entire price of DR. The variation of RS is modelled by the beta and Weibull distributions. Reference [84] formulated a multi-objective optimal allocation model designed for a standalone microgrid system, addressing the conflict issue that arises between the distributed generation owner and the distribution company. In [85], the appropriate allocation, type, and cost of five hybrid storage devices are tested considering the on-grid and islanded microgrid modes of operation. Hussain et al. [86] developed PSO and GA techniques in order to identify the DG size and site within the microgrid cluster operating in islanded mode to reduce load shedding, losses, and voltage deviations. Referring to [87], the PSO and modified Dijkstra algorithms are applied to find the suitable positioning and capacity of energy hubs to satisfy energy demands for the electricity, heat, and cooling of an AMG. The proper location and size of solar and WT plants within AMG, while accounting for the EV load, are demonstrated by the use of a multi-objective ant lion optimiser technique [88] and a multi-objective grey wolf optimisation technique [89]-based bilevel optimisation technique. The purpose of these studies was to reduce both variations in voltage and the energy transmitted to AMGs from the national electric system. In [90], the NSGA III technique is proposed for the proper position of solar energy plants and BESDs in the off-grid network to solve challenges related to economic, technical, and environmental issues.

Research on the optimal siting and rating of DR in DIMG has increased significantly in recent years [30], [91], [92], [93], [94], [95], [96], [97], [98], [99], [100]. A novel mathematical modelling for the planning and management of an IMG's operations was presented in reference [91] through the regionalisation approach to partition the IMG into non-renewable and renewable DG-dominated areas, with the optimal area calculation using the hierarchical clustering technique. Uniyal et al. [92] developed combining a fuzzy approach with the NSGA II algorithm to concurrently optimise the DG’s location in an IMG. The aim was to decrease working voltage and frequency deviation. The MINLP technique is used in [93] to reduce lost active power, and variations in the IMG voltage magnitude and frequency. References in [94], [95] proposed the MILP technique for both optimal DG site capable of injecting/absorbing reactive power and a reconfigurable network in DIMGs in order to minimise active power loss. In [96], a chaotic GWO algorithm is developed to size and place droop and renewable DGs, and CBs within the IMG system to lower losses and increase the VSI of the node. The cost of DG droop fuel, together with overall voltage deviation, and VSI, is optimised as a consequence of the hybrid strategy [97] that incorporates fuzzy technique, harmonic search, and GA to discover the ideal size and location of the IMG system based on fuel and renewable resources. In [98], a hybrid technique combining GA and MINLP is used to find the best allocation of WTs, diesel generations, and compensable capacitor devices within an IMG network to minimise the total price. Reference [99] developed an optimal two-stage model employing a GA algorithm to minimise total cost. In the first one, it allocated power to distributed EBDs for possible island scenarios, while the second stage used sequential Monte Carlo simulation to assess system reliability. Castro et al. [100] presented a hierarchical optimisation approach to manage energy and volt/var control in AMG clusters using decentralised controllers. While central controllers are to determine the boundary of inverter reactive power capability for the grid voltage control.

The appropriate positioning of BESD in IMGs is essential for some reasons: 1) to maintain the microgrid voltage frequency and magnitude in predefined bounds; 2) to optimise energy flow in the system; 3) to efficiently harvest energy from RS; 4) to minimise environmental issues; and more. Many different techniques have been used for the purpose of optimising the site and size of BESD in IMGs, including the PSO algorithm [85], NSGA III [90], teaching learning-based optimisation [101], Bat optimisation algorithm [102], analytical method [103], MILP [104], mixed-integer quadratic programming [105], MOPSO and fuzzy techniques [106], stability and economy-oriented approaches [107].

The stable operation of IMGs that integrate renewable DGs in standard limits is not easy because this electric system does not exist a slack bus. To this end, dump load, CB, STATCOM, etc. can be used. Researchers have also paid great attention to the discussion of the appropriate location and size of dump loads [26], [28], shunt capacitors [108], [109], [110], [111], [112], and STATCOM [113] in IMGs. The strategic site of the shunt capacitors (SC) in IMG is obtained using the HS algorithm that takes into account the demand response [108] and the GA algorithm [109]. The location of the type of switchable and fixed CB (SF) in both the off-grid and on-grid modes of the microgrid is reached using the GA algorithm [110], [112] and the spotted hyena optimiser algorithm [111]. When optimising SC and SF positioning, microgrid energy losses are considerably minimised. In [113] the optimal operation of the STATCOM device in isolated MGs that include WT is proposed to enhance the stable grid against fluctuation of WT.

## 2.2 Related work on the investigation of the effect of deploying multiple Droop-DG sites for islanded AC Microgrid for lost power mitigation

To take advantage of the compact DG size, one shall be deployed in many places (i.e., buses) on the grid. The aim is to maximise the advantages of installing DG, including mitigating transmission and distribution power losses, resulting in increased energy efficiency [33], [114], [115], [116], [117]. Furthermore, this strategy also helps the grid maintain a stable voltage state and contributes to improving its power quality.

DG number and capacity in DN have been examined using distinct techniques, including multi-objective genetic algorithm [118], direct and continuation power flow methods [119], improved analytical method [120], PSO [121], [122], GA tool [123], arithmetic optimisation and Salp swarm algorithms [124], Harris Hawks optimiser [125], GA algorithm [126], plant propagation algorithm [127], improved sine cosine algorithm [128]. The study investigates the deployment of one, two, and three DGs [119], [120], [121], [122], [123], [124], [128], one, two, three, and four DGs [125], [126], [127], ten DGs [122], and greater than 30% of all system buses [114], [115], [116], [117].

In IMG networks that are no droop-based, multiple DG sites can be deployed in order to mitigate energy losses, in accordance with Refs. [33], [80], [81], [83], [86], as described in Section 2.1 of Chapter 2. For this approach, existing DNs are transformed into autonomous network topologies. Afterward, the identification process is conducted to properly place the DGs on the investigated grid. Furthermore, Sivakumar et al. [117] also suggested bi-direct load flow and lost active power sensitivity approaches to the size of fuel and renewable DGs in non-droop microgrid clusters operating in on-grid and isolated modes.

The DG siting and/or capacity in IMGs using the droop strategy are also detailed in the references mentioned above, as presented in Section 2.1 of Chapter 2. The primary purpose of these works was to lower lost power and improve bus voltage magnitudes.

## 2.3 Conclusion

The literature survey is provided in Section 2.1, which focusses on the optimal allocation and location of DR units, dump loads and VAR compensable devices in IMGs, integrating the problem of economic dispatch, environmental issues, demand side management, and optimal operation. The purpose of these works is to enhance the operational capacity of the IMG grid, mitigate environmental pollutants, and be economically optimal. As mentioned in [5], no algorithm can ever fully resolve all optimisation problems. Therefore, it is imperative to develop and/or apply an effective algorithm to tackle the ideal droop-DG allocation within the IMG for maximum benefits of installing this generator on the grid, as expressed in more detail in Section 1.1 of Chapter 1. In this thesis, the new honey badger-based metaheuristic algorithm is applied to deal with the problem mentioned above.

Section 2.2 reviews existing studies related to the problem of installing a number of droop-DG locations in DNs both in the on-grid and islanded modes to maximise lost power reduction. The analysis of the above-mentioned literature, which is summarised in Table 2. 1, points out a knowledge gap: There is a lack of research to investigate the impact of optimally placing multiple droop-DGs in an islanded microgrid to significantly minimise power loss in lines, as well as bus voltage improvement. Therefore, this thesis also addresses the aforementioned gap. This work develops a differential evolution algorithm along with the MBFS load flow approach to find the appropriate multiple droop-DG sites in IMGs to maximise the extent of minimising lost power and gain bus voltage.

Table 2. 1 Summarising literature, highlighting key contributions of the work

| Ref. | Year | On-grid | Off-grid | Droop control | $P_{loss}$ reduction | $Q_{loss}$ reduction | Optimal P and/or S | Investigate the effect of placing multiple DG sites |
|---|---|---|---|---|---|---|---|---|
| [120] | 2011 | C | | | C | | P and S | C |
| [33] | 2012 | | C | | C | C | P and S | C |
| [114] | 2014 | C | | | C | C | P and S | C |
| [80] | 2015 | C | C | | C | | P and S | C |
| [121] | 2016 | C | | | C | | P and S | C |
| [97] | 2016 | | C | C | C | C | P and S | |
| [96] | 2017 | | C | C | C | C | P and S | |
| [48] | 2017 | | C | C | C | C | S | |
| [101] | 2018 | | C | | C | | P and S | |
| [81] | 2019 | C | C | | C | C | P and S | C |
| [123] | 2019 | C | | | C | | P and S | C |
| [94] | 2020 | | C | C | C | C | P and S | |
| [127] | 2020 | C | | | C | | P and S | C |
| [98] | 2020 | | C | C | C | C | P and S | |
| [43] | 2021 | | C | C | C | | S | |
| [46] | 2021 | | C | C | C | C | S | |
| [44] | 2021 | | C | C | C | | S | |
| [93] | 2021 | | C | C | C | | P and S | |
| [39] | 2021 | | C | | | | P and S | C |
| [117] | 2021 | C | C | | C | | P and S | |
| [124] | 2022 | C | | | C | | P and S | C |
| [125] | 2022 | C | | | C | C | P and S | C |
| [122] | 2023 | C | | | C | C | P and S | C |
| [129] | 2023 | | C | C | C | C | P and S | |
| **This study** | | | **C** | **C** | **C** | **C** | **C** | **C** |

$P_{loss}$–lost active power, $Q_{loss}$–lost reactive power, P–positioning, S–size, C–consider

# CHAPTER

# 3

# METHODOLOGIES FOR THE OPTIMAL ALLOCATION OF DROOP-DG IN ISLANDED AC MICROGRID

In this doctoral thesis, robust methodologies are proposed to resolve the proper allocation and site of droop-DGs in IMGs to minimise lost power and gain bus voltage and voltage stability margin. Specifically, DE and HB techniques are applied to tune control variables (i.e., droop parameters and droop-DG site), while the suggested MBFS load flow approach is used to find optimal operational points and satisfy constraint conditions. Furthermore, a mathematical model formulation for tuning the droop parameters of droop-DGs in IMGs is also presented.

## 3.1 Differential evolution technique

The DE technique is a global optimisation method that is conducted iteratively by evolving a population solution. It has been designed in order to resolve real applications. One of the conveniences of this algorithm is that the initial inhabitants (i.e., the population) can be generated through a random technique without requiring knowledge about the objective function. Inhabitants of the DE algorithm can be formed,

$$\boldsymbol{Z_D} = \begin{bmatrix} z_{11} & z_{12} & \dots & z_{1j} \\ z_{21} & z_{22} & \dots & z_{2j} \\ \dots & & \dots & \\ z_{i1} & z_{i2} & \dots & z_{ij} \end{bmatrix}, \quad i \in [1, S_D] \cap Z, \quad j \in [1, D_D] \cap Z \tag{3.1}$$

where: $\boldsymbol{Z_D}$ denotes candidate solution habitants; $S_D$ represents the size of habitants; $D_D$ signifies the dimensional vectors of the control variables; $Z$ denotes a numerical integer.

The following describes the performance phases of the DE algorithm [130].

**Phase 1:** Initial inhabitants can be generated in the first generation ($g$=0). The elements of the initial inhabitants can be ascertained as

$$z_{ij}^{0} = bound_{j,B} + \text{rand}_j(0,1)\,(bound_{j,T} - bound_{j,B}) \tag{3.2}$$

where: $bound_{j,B}$ and $bound_{j,T}$ comprise the bottom and top thresholds of the $j$-th control variable respectively while $\text{rand}_j(0, 1)$ represents a randomness number of the $j$-th control variable that falls between [0, 1).

**Phase 2:** Reassembling random components from three distinct population solution vectors including $\boldsymbol{z_{c1}^{g}}, \boldsymbol{z_{c2}^{g}},$ and $\boldsymbol{z_{c3}^{g}}$ yields the mutation vector $\boldsymbol{v_i^{g}}$ in each $g$-th generation. Equation (3.3) presents the DE/rand/1/bin-based mutation strategy [131].

$$\boldsymbol{v_i^{g}} = \boldsymbol{z_{c3}^{g}} + F(\boldsymbol{z_{c1}^{g}} - \boldsymbol{z_{c2}^{g}}), \quad i \in [1, S_D] \cap Z, \quad g \in [1, G_{\max}] \cap Z \tag{3.3}$$

where: $F$ signifies the scaling factor $\in [0, 2]$, higher values of $F$ point out better exploration throughout the search space. In contrast, smaller values of $F$ boost a faster speed of convergence [132]; the highest generation count is represented by $G_{\max}$; the values of $c1$, $c2$, and $c3$ are various randomised positive integer indices $\in [1, S_D]$, where $S_D \geq 4$.

The various types of mutation strategies of the DE algorithm are presented below [131]:

- Mutation strategy 1–DE/rand/2/bin

$$\boldsymbol{v}_{i}^{g} = \boldsymbol{z}_{c1}^{g} + F(\boldsymbol{z}_{c2}^{g} - \boldsymbol{z}_{c3}^{g}) + F(\boldsymbol{z}_{c4}^{g} - \boldsymbol{z}_{c5}^{g}) \tag{3.4}$$

- Mutation strategy 2–DE/best/1/bin

$$\boldsymbol{v}_{i}^{g} = \boldsymbol{z}_{best} + F(\boldsymbol{z}_{c1}^{g} - \boldsymbol{z}_{c2}^{g}) \tag{3.5}$$

- Mutation strategy 3–DE/best/2/bin

$$\boldsymbol{v}_{i}^{g} = \boldsymbol{z}_{best} + F(\boldsymbol{z}_{c1}^{g} - \boldsymbol{z}_{c2}^{g}) + F(\boldsymbol{z}_{c3}^{g} - \boldsymbol{z}_{c4}^{g}) \tag{3.6}$$

- Mutation strategy 4–DE/current to best/1

$$\boldsymbol{v}_{i}^{g} = \boldsymbol{z}_{i}^{g} + F(\boldsymbol{z}_{best} - \boldsymbol{z}_{i}^{g}) + F(\boldsymbol{z}_{c1}^{g} - \boldsymbol{z}_{c2}^{g}) \tag{3.7}$$

- Mutation strategy 5–DE/current to rand/1

$$\boldsymbol{v}_{i}^{g} = \boldsymbol{z}_{i}^{g} + F(\boldsymbol{z}_{c1}^{g} - \boldsymbol{z}_{i}^{g}) + F(\boldsymbol{z}_{c2}^{g} - \boldsymbol{z}_{c3}^{g}) \tag{3.8}$$

where: the different random integer indices $c1$, $c2$, $c3$, $c4$, and $c5$ are within the range of [1, $S_D$]; $\boldsymbol{z}_{best}$ represents the best inhabitant in the population up to the $g$ - th generation.

The DE/rand/1/bin and DE/rand/2/bin mutation strategies have been applying for many real-world applications due to their ability to find out new inhabitants throughout the search process. However, the exploitability of these two strategies is low. The advantage of strategies 2 and 3 is a rapid convergence speed toward the global optimal. Nevertheless, the previously mentioned two mutation techniques lack the exploration capability in the inhabitants. Also, leaving a local extreme is hard. To overcome the shortcomings of the DE algorithm's mentioned strategies, strategies 4 and 5 are developed to balance its exploration and exploitation ability.

**<u>Phase 3</u>:** The DE algorithm uses the crossover operator in order to produce new inhabitants by modifying the mutant vector. This process increases the multiplicity of population solutions, and the trial vector is shown by

$$\boldsymbol{u_i^g} = (u_{i1}^g,\ u_{i2}^g, \ldots,\ u_{ij}^g), \quad j \in [1,\ D_D] \cap Z \tag{3.9}$$

It can be expressed as follows:

$$u_{ij}^g = \begin{cases} v_{ij}^g & \text{if } j \in [1,\ D_D] \cap Z \ \text{ or } \ r_j(0,\ 1) \le CR \\ z_{ij}^g & \text{otherwise} \end{cases} \tag{3.10}$$

where: $r_j(0,\ 1)$ denotes a uniform randomness number while $CR$ represents the crossover factor, and its best values range 0.4–1.0 [133].

**<u>Phase 4</u>:** Comparing the respective fitness values of solutions $\boldsymbol{u_i^g}$ and $\boldsymbol{z_i^g}$ is in order to update an inhabitant for the subsequent generation. For a minimisation problem, the solution (i.e., inhabitant) with the lower fitness value is chosen and given by

$$\boldsymbol{z_i^g} = \begin{cases} \boldsymbol{u_i^g} & \text{if } f\ (\boldsymbol{u_i^g}) \le f\ (\boldsymbol{z_i^g}) \\ \boldsymbol{z_i^g} & \text{otherwise} \end{cases}, \quad f() \text{ denotes the fitness} \tag{3.11}$$

## 3.2 Honey badger technique

The HB technique draws inspiration from the hunting habits of honey badgers in the wild. This algorithm has been applied in practice because of its balance in exploration and exploitation. This equilibrium is essential for metaheuristic-based techniques, such as the HB algorithm. Therefore, the HB algorithm is able to adapt to complex search spaces in order to identify optimal solutions.

The inhabitants $\boldsymbol{H_H}$ of the HB algorithm are defined in a matrix below.

$$\boldsymbol{H_H} = \begin{bmatrix} h_{11} & h_{12} & \ldots & h_{1j} \\ h_{21} & h_{22} & \ldots & h_{2j} \\ \ldots & & \ldots & \\ h_{i1} & h_{i2} & \ldots & h_{ij} \end{bmatrix}, \quad i \in [1, S_H] \cap Z, \quad j \in [1, D_H] \cap Z \tag{3.12}$$

where: $S_H$ denotes the population's size; $D_H$ signifies dimensional search area; $Z$ signifies a numerical integer.

The sequential performance of the HB technique is represented as follows [13]:

**Phase 1:** Generate the first honey badger site with the inhabitants' size $S_H$ based on equation (3.13):

$$\boldsymbol{h_i} = \boldsymbol{r_1}\left(\boldsymbol{UB_i} - \boldsymbol{LB_i}\right) + \boldsymbol{LB_i} \tag{3.13}$$

where: the vectors $\boldsymbol{UB_i}$ and $\boldsymbol{LB_i}$ represent the search space's upper and lower ranges; and the vector $\boldsymbol{r_1}$ denotes a random number $\in (0, 1)$.

**Phase 2:** The mobility of honey badgers to find prey depends on how well the prey scents. Intensity denotes a factor that concerns the prey's level of focus and its length from the HB. The badger's movement will be faster if its smell intensity is strong, and slower if its smell intensity is low. The odour intensity $I_i$ can be calculated by

$$I_i = r_2 \frac{S}{4\pi d_i^2}, \quad r_2 \text{ denotes a random value } \in (0,1) \tag{3.14}$$

$$S = (\boldsymbol{h_i} - \boldsymbol{h_{i+1}})^2 \tag{3.15}$$

$$\boldsymbol{d_i} = \boldsymbol{h_{prey}} - \boldsymbol{h_i} \tag{3.16}$$

where: $S$ represents source strength (i.e., a prey siting); the vector $\boldsymbol{d_i}$ signifies a length calculated from the prey to the $i$-th HB; the vector $\boldsymbol{h_{i+1}}$ denotes the $(i+1)$-th HB siting; and the vector $\boldsymbol{h_{prey}}$ represents a prey placement.

**Phase 3**: To ensure an easy transition from the exploration step to the exploitation step, the density factor $\alpha$ is used. The value of $\alpha$ decreases randomly over time as the number of iterations increases.

$$\alpha = Ce^{-\frac{it}{IT_{\max}}}, \quad it \in [1, IT_{\max}] \cap Z \tag{3.17}$$

where: $C$ is a real constant and $C \geq 1$ (its default value with $C = 2$); the iteration in use represents *it;* the highest iteration count is denoted by $IT_{\max}$.

**Phase 4:** The HB technique uses a digging phase (i.e., a digging technique) or a honey phase (i.e., a honey technique) to create a new position for the $i$-th honey badger. The details of these two phases can be clarified as follows.

**Phase 4-1**: In the digging technique, the badger moves in a similar way to the cardioid shape. The honey badger's movement can be described by

$$\boldsymbol{h}_{i,update}^{it} = \boldsymbol{h}_{prey} + F\beta I\boldsymbol{h}_{prey} + Fr_3\alpha\boldsymbol{d}_i\left|\cos 2\pi r_4[1-\cos(2\pi r_5)]\right| \quad (3.18)$$

$$F = \begin{cases} 1 & \text{if } r_6 \leq 0.5 \\ -1 & \text{otherwise} \end{cases}, \quad r_6 \text{ signifies a random value } \in (0,\ 1) \quad (3.19)$$

where: at the $it$-th iteration, the vector $\boldsymbol{h}_{i,update}^{it}$ shows an updated position of the $i$-th HB; $F$ acts as a flag that aims to select the badger's movement direction; $\beta$ represents the badger's capacity to seek for food and $\beta \geq 1$ (default value with $\beta = 6$ ); $I$ is the level of the odour intensity; $r_3$, $r_4$, and $r_5$ denote distinct random values $\in (0,\ 1)$.

**Phase 4-2**: The following is another approach that is used to update the new siting of the badger, which is aided in its food search by a honeyguide bird and is known as the honey technique.

$$\boldsymbol{h}_{i,update}^{it} = \boldsymbol{h}_{prey} + Fr_7\alpha\boldsymbol{d}_i, \quad r_7 \text{ represents a randomness value } (0 < r_7 < 1) \quad (3.20)$$

**Phase 5**: In order to calculate the fitness value $f_{update}$ of an updated candidate solution $\boldsymbol{h}_{i,update}^{it}$ and compare it with the fitness value $f_i$ of a present solution $\boldsymbol{h}_i^{it}$. For a problem concerning minimisation, if $f_{update} \leq f_i$ then substitute $\boldsymbol{h}_i^{it} = \boldsymbol{h}_{i,update}^{it}$ and $f_i = f_{update}$.

**Phase 6**: If $f_{update} \le f_i$ then compare the fitness values $f_{update}$ and $f_{prey}$, where $f_{prey}$ represents the fitness value of a solution $\boldsymbol{h_{prey}}$. If $f_{update} \le f_{prey}$ then substitute $\boldsymbol{h_{prey}} = \boldsymbol{h_{i,update}^{it}}$ and $f_{prey} = f_{update}$.

**Phase 7**: In order to verify the stopping criterion, if not met, subsequently redo from Phase two through Phase six; otherwise, print the best objective function/fitness $f_{prey}$, together with its solution $\boldsymbol{h_{prey}}$.

## 3.3 Optimal power flow within a DIMG

Optimal Power Flow is a computational technique that optimises the setting of decision variables like generator output, transformer and voltage regulator taps, etc. to reduce production power costs, operating and maintenance costs while ensuring operational efficiency and reliable grid. In the operation of DIMG systems, it is essential to optimise the calculation of energy flow within the grid, contributing to efficient resource use, increasing grid stability, and improving power quality.

### 3.3.1 Electric load modelling

The electric load's power consumption depends on the working voltage magnitude and frequency. Therefore, a static load model in [134] is taken into account for the shift in bus power regarding nodal voltage variation, specifically $P_{Li}$ and $Q_{Li}$, is determined by

$$\begin{aligned} P_{Li} &= P_{Lio}\left(\frac{|V_i|}{|V_o|}\right)^p \left(1 + K_{pf}(f - f_o)\right) \\ Q_{Li} &= Q_{Lio}\left(\frac{|V_i|}{|V_o|}\right)^q \left(1 + K_{qf}(f - f_o)\right) \end{aligned} \tag{3.21}$$

where: $P_{Lio}$ and $Q_{Lio}$ denote the power consumption at the device's rated voltage value; $|V_i|$ signifies the working voltage magnitude, while $|V_o|$ represents the device's rated voltage magnitude; $f_o$ signifies the rated frequency; $f$ denotes the working frequency; $p$ and $q$ are the exponent values; $K_{pf}$ and $K_{qf}$ represent the frequency sensitivity parameters.

### 3.3.2 DG model functioning in a DIMG

In cutting-edge electric power systems like microgrids, DGs equipped with inverter interfaces are preferred to be installed due to their advantages. One of these advantages is compact size, quick response to power grid fluctuations arising from RS and load variations, and the ability to gain the system dependability and stability throughout the operating process.

Inverter-based DG is offered by two modes of functioning as follows [135]:

- PQ inverter control mode: In this mode, the DG can provide/draw predetermined active and reactive powers to/from the electric system.
- Voltage source inverter control mode: In this scenario, the DG acts as synchronous generators, utilised to control the working voltage magnitude and frequency using droop operation.

The inverter-based DG's mathematical model, operating in an IMG through the droop law, depends on the impedance $Z$ that encompasses the DG internal impedance and the impedance along the lines that link the DG to the power grid, as illustrated in Fig. 3. 1 [136].

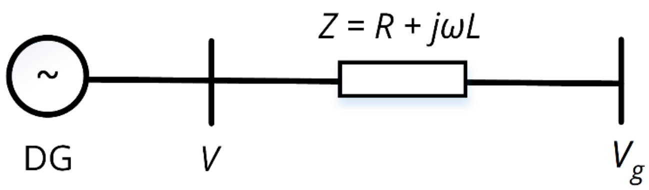


Fig. 3. 1 Inverter-based DG linking to the power grid

where: $V$ denotes the DG terminal voltage; $V_g$ represents the grid voltage; $Z$ signifies the equivalent impedance.

The following expresses the droop equations of the DG within IMG networks depending on the impedance $Z$:

When the impedance's value $Z$ is a predominant resistance. That is, the DG internal impedance is greatly resistive. Furthermore, the impedance of the line is mainly resistive. Therefore, the droop strategy with the impedance of the predominant resistance can be expressed by [137], [138]

$$f = f_o + m_p(Q_{DG} - Q_{DGo}) \tag{3.22}$$

$$|V| = |V_{ref}| - n_q(P_{DG} - P_{DGo}) \tag{3.23}$$

where: $P_{DG}$ and $Q_{DG}$ signify the DG production power; $P_{DGo}$ and $Q_{DGo}$ denote the power reference points of the DG [23], and have the option to be set to zero [139]; $m_p$ and $n_q$ are the $P$ and $Q$ droop gains of the DG while $|V_{ref}|$ and $|V|$ are its reference and terminal voltage magnitudes; $f_o$ signifies the set frequency; $f$ represents the working voltage's frequency.

When the value of the impedance $Z$ is a predominant inductance. In other words, the internal impedance of the DG is mostly inductive and the impedance of the line is also primarily inductive [136], [140]. As a result, the droop technique based on the predominant inductance impedance is determined as in equations (3.24) and (3.25) [23]**:**

$$f = f_o + m_p(P_{DG} - P_{DGo}) \tag{3.24}$$

$$|V| = |V_{ref}| + n_q(Q_{DG} - Q_{DGo}) \tag{3.25}$$

In practice, to improve the control quality of the DG droop strategy in microgrids, it is crucial to note that the considered impedance $Z$ should consist of resistive and inductive components and is called a complex impedance. At that time, the frequency and magnitude of the grid voltage are simultaneously influenced by the active and reactive production power of DG. Consequently, the complex impedance-based droop equations are given as [136]

$$f = f_o - m_p(P_{DG} - Q_{DG}) \tag{3.26}$$

$$|V| = |V_{ref}| - n_q(P_{DG} + Q_{DG}) \tag{3.27}$$

### 3.3.3 MBFS load flow method in a DIMG

The noticeable feature of operating microgrids in an islanded mode does exist no slack bus. This results from using compact-size dispersed and/or distributed generators (DG) to create potential benefits of deploying DGs. As a result, the must-have condition of having at least one DG uses the droop law to regulate the IMG voltage and frequency inside the intended bounds [43].

The MBFS approach is applicable to calculate the energy flow within the DIMGs mentioned above. This algorithm can be partitioned into the following four phases: first, an initialisation phase is performed for the installation of the initial parameters of the system; second, a backward sweep is used to calculate the apparent power and current injected at every bus, as well as the branch current; third, a forward sweep is employed to determine the bus voltage that excludes a virtual bus (VB); and finally, the update phase corrects the VB voltage and frequency values, the power injection of all DG buses, and the branch impedances.

The following describes the phases of the MBFS approach [23]:

***Phase 1: Initial Phase***

Presuming the presence of one swing bus (slack bus) within a DIMG system, we should regulate the slack bus's voltage and the operating frequency so that power intake fed into the slack bus is zero, while maintaining them inside a permissible threshold. This bus is considered the virtual bus. To reduce the use of computer resources, the first node is often designated as the swing bus.

Initial settings comprise the following parameters: set the working frequency $f = 1$ pu and the voltage of all microgrid buses $V_i = 1\angle 0^o$ pu; the VB's voltage deviation $\Delta V_1 = 0$; the microgrid's frequency deviation $\Delta f = 0$; outer and inner iteration counters $u$ and $w$ are equal to 0; tolerance limits $\varepsilon_i = \varepsilon_o = 10^{-4}$.

In the MBFS method, the DG model using the droop law based on equations (3.24) and (3.25) is used. To minimise deviations in IMG frequency and voltage, islanded DG output power must be adjusted at a suitable level, and determined by

$$P_{DGi} = P_{DGio} + \Delta P_{DGi}, \qquad \Delta P_{DGi} = \frac{\Delta f}{m_{pi}}, \qquad \Delta f = f - f_o \tag{3.28}$$

$$Q_{DGi} = Q_{DGio} + \Delta Q_{DGi}, \qquad \Delta Q_{DGi} = \frac{\Delta V_i}{n_{qi}}, \qquad \Delta V_i = |V_i| - 1 \tag{3.29}$$

where: $i \in [1, N] \cap Z, N$ represents the IMG's number of buses/nodes while $Z$ signifies a numerical integer; the production power of droop-DG at node $i$ is denoted by $P_{DGi}$ and $Q_{DGi}$; the power reference points of DG at bus $i$ are expressed by $P_{DGio}$ and $Q_{DGio}$; $\Delta P_{DGi}$ and $\Delta Q_{DGi}$ are the production power given by droop-DG at node $i$ to decrease the IMG's power mismatches; the DG terminal voltage deviation at bus $i$ is signified by $\Delta V_i$; the $f$ and $V$ droop gains of DG at node $i$ are represented by $m_{pi}$ and $n_{qi}$; the value of the reference frequency $f_o$ is set at 1.0

***Phase 2: Backward sweep***

The apparent power and current $S_i$ and $I_i$ injected at every node can be computed through equations (3.30) and (3.31) when the load and DG power values, as well as the bus voltage, are known.

$$\begin{aligned} S_i &= P_i + jQ_i \\ P_i &= P_{Li} - P_{DGi} \\ Q_i &= Q_{Li} - Q_{DGi} \end{aligned} \tag{3.30}$$

$$I_i = \left(\frac{S_i}{V_i}\right)^*, \quad i \in [2, N] \cap Z \tag{3.31}$$

Determining the vector of branch current $\boldsymbol{B_{branch}}$ through the bus current vector $\boldsymbol{I_{bus}}$ and the matrix of bus-injection to branch-current $\boldsymbol{BIBC}$ is as

$$[\boldsymbol{B_{branch}}] = [\boldsymbol{BIBC}][\boldsymbol{I_{bus}}] \tag{3.32}$$

In radial microgrids, the matrix $\boldsymbol{BIBC}$ can be computed as in [141], [142].

***Phase 3: Forward sweep***

In this phase, the new values of the bus voltage from the second bus to the last bus can be updated as in equation (3.33) through the VB's voltage vector $\boldsymbol{V_1}$, the branch current vector $\boldsymbol{B_{branch}}$, and the branch current to bus voltage matrix $\boldsymbol{BCBV}$.

$$[\boldsymbol{V}] = [\boldsymbol{V_1}] - [\boldsymbol{BCBV}][\boldsymbol{B_{branch}}] \tag{3.33}$$

In radial microgrids, the transformation matrix $\boldsymbol{BCBV}$ can be determined as follows [142]:

$$[\boldsymbol{BCBV}] = [\boldsymbol{BIBC}]^{\boldsymbol{T}} diag[\boldsymbol{Z_{branch}}] \tag{3.34}$$

where: $\boldsymbol{BIBC^T}$ denotes an inverse of the matrix $\boldsymbol{BIBC}$; $\boldsymbol{Z_{branch}}$ signifies the branch impedance matrix.

The following equation is applied to compute the voltage tolerance value $TOL$ for the convergence criterion in order to stop the $w$-th inner iteration.

$$TOL = \max |V_i^w - V_i^{w-1}|, \quad i \in [2, N] \cap Z \tag{3.35}$$

where: $|V_i^w|$ and $|V_i^{w-1}|$ signify the voltage's magnitudes at node $i$ during the inner iterations $w$ and $(w-1)$.

***Phase 4: Updated Phase***

If the tolerance $TOL$ value is below the threshold value $\varepsilon_i$, the VB voltage frequency and magnitude are updated according to equations (3.36) and (3.39).

$$f^{u+1} = f^u + \Delta f \tag{3.36}$$

$$\Delta f = m_{pE}[P_{DG1} - \Re(V_1 B_{j-1}^{\ *})] \tag{3.37}$$

$$m_{pE} = \left( \sum_{i=1}^{N_{DG}} \frac{1}{m_{pi}} \right)^{-1} \tag{3.38}$$

where: $f^{u+1}$ and $f^{u}$ are the IMG's operating frequency during both the $(u+1)$-th and $u$-th outer iterations; $m_{pE}$ denotes the equivalent $f$ droop coefficient; $P_{DG1}$ signifies the power yielded by DG in the VB; $\Re(V_1 B_{j-1}^{*})$ represents a real component of the apparent power that flows to the $j$-th node from the VB.

$$|V_1^{u+1}| = |V_1^{u}| + \Delta V_1 \tag{3.39}$$

$$\Delta V_1 = n_{qE}[Q_{DG1} - \Im(V_1 B_{j-1}^{*})] \tag{3.40}$$

$$n_{qE} = \left( \sum_{i=1}^{N_{DG}} \frac{1}{n_{qi}} \right)^{-1} \tag{3.41}$$

where: $|V_1^{u+1}|$ and $|V_1^{u}|$ are the VB's voltage magnitudes during both the $(u+1)$-th and $u$-th outer iterations; $n_{qE}$ is the equivalent $V$ droop coefficient; $Q_{DG1}$ represents the power yielded by DG in the VB; $\Im(V_1 B_{j-1}^{*})$ denotes an imaginary component of the apparent power that flows to the $j$-th node from the VB.

The DG's output power is updated according to equations (3.42) and (3.43).

$$P_{DGi} = P_{DGio} + \frac{\Delta f}{m_{pi}} \tag{3.42}$$

$$Q_{DGi} = Q_{DGio} + \frac{\Delta V_i}{n_{qi}} \tag{3.43}$$

The microgrid's branch impedances should be updated as

$$Z_{ij} = R_{ij} + jX_{ij} \frac{f^{u+1}}{f^{u}} \tag{3.44}$$

If the value of $\Delta V_1$ in equation (3.40) is below the limit value $\varepsilon_o$, the MBFS algorithm is over.

### 3.3.4 Optimisation droop parameters of dispatchable droop-DGs

Within the islanded working of microgrids, the power sharing among droop-DGs is proposed. Real power sharing is tuned by $m_{pi}$ while sharing reactive power is performed by $n_{qi}$ and $|V_{refi}|$. The mathematical formulation of the DG droop parameters in an IMG is expressed, where the author of this doctoral thesis modifies the proposed equations from references [44], [48]. Specifically, the mathematical model formulation for tuning droop parameters of DGs consists of the power set points $P_{DGio}$ and $Q_{DGio}$, is described as follows:

Under no-load functioning conditions, the frequency of each droop-DG is the same. From equation (3.24), we can write below

$$P_{DGi}^{s} = \frac{f^{s} - f_{ref}}{m_{pi}} + P_{DGio}, \quad s \in [1, S] \cap Z \tag{3.45}$$

where: $P_{DGi}^{s}$ is the DG's active production power at the $i$-th bus in scenario $s$; $f^{s}$ is the IMG's operating frequency in scenario $s$; $f_{ref}$ signifies the reference frequency; $s$ denotes the investigated scenario; $S$ is the total studied scenarios; $Z$ signifies a numerical integer.

When the IMG frequency functions at the lowest permissible threshold, the DGs will provide rated active powers.

$$P_{DGi}^{rated} = \frac{f^{\min} - f_{ref}}{m_{pi}} + P_{DGio} \tag{3.46}$$

where: $P_{DGi}^{rated}$ is the DG's rated active power at the $i$-th bus; $f^{\min}$ represents the minimum frequency threshold.

From equation (3.45), we can acquire:

$$\sum_{i=1}^{N_{DG}} P_{DGi}^{s} = (f^{s} - f_{ref}) \sum_{i=1}^{N_{DG}} \frac{1}{m_{pi}} + \sum_{i=1}^{N_{DG}} P_{DGio} \tag{3.47}$$

From equation (3.46), we can get:

$$\sum_{i=1}^{N_{DG}} P_{DGi}^{rated} = \sum_{i=1}^{N_{DG}} \left( \frac{f^{\min} - f_{ref}}{m_{pi}} + P_{DGio} \right) = \Delta f^{\max} \sum_{i=1}^{N_{DG}} \frac{1}{m_{pi}} + \sum_{i=1}^{N_{DG}} P_{DGio}, \text{ with } \Delta f^{\max} = f^{\min} - f_{ref} \tag{3.48}$$

where: the maximum permitted frequency deviation is denoted by $\Delta f^{\max}$.

Dividing equation (3.45) by equation (3.47) yields:

$$\frac{P_{DGi}^{s}}{\sum_{i=1}^{N_{DG}} P_{DGi}^{s}} = \frac{\frac{1}{m_{pi}}(f^{s} - f_{ref}) + P_{DGio}}{(f^{s} - f_{ref})\sum_{i=1}^{N_{DG}} \frac{1}{m_{pi}} + \sum_{i=1}^{N_{DG}} P_{DGio}} \tag{3.49}$$

From equation (3.48), we obtain:

$$\sum_{i=1}^{N_{DG}} \frac{1}{m_{pi}} = \frac{\sum_{i=1}^{N_{DG}} P_{DGi}^{rated}}{\Delta f^{\max}} - \frac{\sum_{i=1}^{N_{DG}} P_{DGio}}{\Delta f^{\max}} \tag{3.50}$$

By substituting $\sum_{i=1}^{N_{DG}} \frac{1}{m_{pi}}$ in equation (3.50) into equation (3.49), we get:

$$\frac{P_{DGi}^{s}}{\sum_{i=1}^{N_{DG}} P_{DGi}^{s}} = \frac{\frac{1}{m_{pi}}(f^{s} - f_{ref}) + P_{DGio}}{\frac{(f^{s} - f_{ref})}{\Delta f^{\max}}\left(\sum_{i=1}^{N_{DG}} P_{DGi}^{rated} - \sum_{i=1}^{N_{DG}} P_{DGio}\right) + \sum_{i=1}^{N_{DG}} P_{DGio}} \tag{3.51}$$

We can infer the value of $m_{pi}$ from equation (3.51) as follows:

$$m_{pi} = \frac{(f^{s} - f_{ref})}{\frac{P_{DGi}^{s}}{\sum_{i=1}^{N_{DG}} P_{DGi}^{s}}\left[\frac{(f^{s} - f_{ref})}{\Delta f^{\max}}\left(\sum_{i=1}^{N_{DG}} P_{DGi}^{rated} - \sum_{i=1}^{N_{DG}} P_{DGio}\right) + \sum_{i=1}^{N_{DG}} P_{DGio}\right] - P_{DGio}} \tag{3.52}$$

If the value of $P_{DGio} = 0,$ equation (3.52) can be rewritten:

$$m_{pi} = \frac{\Delta f^{\max}}{\sum_{i=1}^{N_{DG}} P_{DGi}^{rated}} \frac{\sum_{i=1}^{N_{DG}} P_{DGi}^{s}}{P_{DGi}^{s}} \tag{3.53}$$

The tuning value of $m_{pi}$ can be computed through the known value of the active power sharing ratio $\frac{\sum_{i=1}^{N_{DG}} P_{DGi}^{s}}{P_{DGi}^{s}}$, as described in equation (3.52). To explain further, if the active power sharing ratio between droop-DGs is found then the value of $m_{pi}$ can be calculated.

Under no-load functioning conditions, the terminal voltage of each droop-DG is distinct. Based on equation (3.25), we can then write as

$$Q_{DGi}^{s} = \frac{|V_i^{s}| - |V_{refi}|}{n_{qi}} + Q_{DGio} \tag{3.54}$$

where: $Q_{DGi}^{s}$ represents the DG's reactive production power at node $i$ within scenario $s$; $|V_i^{s}|$ denotes the DG terminal voltage magnitude at node $i$ within scenario $s$, while $|V_{refi}|$ signifies its reference voltage magnitude.

When the IMG voltage functions at the lowest predetermined value, the DGs will also supply rated reactive powers, described as in equation (3.55).

$$\begin{aligned} Q_{DGi}^{rated} &= \frac{|V_i^{\min}| - |V_{refi}|}{n_{qi}} + Q_{DGio} \\ &= \frac{\Delta |V_i^{\max}|}{n_{qi}} + Q_{DGio}, \text{ with } \Delta |V_i^{\max}| = |V_i^{\min}| - |V_{refi}| \end{aligned} \tag{3.55}$$

where: $Q_{DGi}^{rated}$ is the DG's rated reactive production power at bus $i$; $\Delta |V_i^{\max}|$ represents the maximum permitted node voltage deviation.

From equation (3.54), we can acquire:

$$\sum_{i=1}^{N_{DG}} Q_{DGi}^{s} = \sum_{i=1}^{N_{DG}} \frac{|V_i^s| - |V_{refi}|}{n_{qi}} + \sum_{i=1}^{N_{DG}} Q_{DGio} \tag{3.56}$$

Dividing equation (3.54) by equation (3.56) yields:

$$\frac{Q_{DGi}^{s}}{\sum_{i=1}^{N_{DG}} Q_{DGi}^{s}} = \frac{\frac{1}{n_{qi}}(|V_i^s| - |V_{refi}|) + Q_{DGio}}{\sum_{i=1}^{N_{DG}} \frac{|V_i^s| - |V_{refi}|}{n_{qi}} + \sum_{i=1}^{N_{DG}} Q_{DGio}} \tag{3.57}$$

From equation (3.55), we obtain:

$$\frac{1}{n_{qi}} = \frac{Q_{DGi}^{rated} - Q_{DGio}}{\Delta |V_i^{\max}|} \tag{3.58}$$

Substituting $\frac{1}{n_{qi}}$ in equation (3.58) into equation (3.57), we acquire:

$$\frac{Q_{DGi}^{s}}{\sum_{i=1}^{N_{DG}} Q_{DGi}^{s}} = \frac{\frac{Q_{DGi}^{rated} - Q_{DGio}}{\Delta |V_i^{\max}|}(|V_i^s| - |V_{refi}|) + Q_{DGio}}{\sum_{i=1}^{N_{DG}} \frac{|V_i^s| - |V_{refi}|}{n_{qi}} + \sum_{i=1}^{N_{DG}} Q_{DGio}} \tag{3.59}$$

If $Q_{DGio} = 0$, equation (3.59) can be rewritten as

$$\frac{Q_{DGi}^{s}}{\sum_{i=1}^{N_{DG}} Q_{DGi}^{s}} = \frac{Q_{DGi}^{rated}}{\Delta |V_i^{\max}|} \frac{(|V_i^s| - |V_{refi}|)}{\sum_{i=1}^{N_{DG}} \frac{|V_i^s| - |V_{refi}|}{n_{qi}}} \tag{3.60}$$

The optimal value of the power sharing ratio $\frac{Q_{DGi}^{s}}{\sum_{i=1}^{N_{DG}} Q_{DGi}^{s}}$ in equation (3.59) is known.

By tuning the droop parameters $n_{qi}$ and $|V_{refi}|$ be inside the set ranges $[n_{qi}^{\min}, n_{qi}^{\max}]$ and $[|V_{refi}^{\min}|, |V_{refi}^{\max}|]$ respectively, we must ascertain the correct value of

$\dfrac{(|V_i^s| - |V_{refi}|)}{\sum_{i=1}^{N_{DG}} \dfrac{|V_i^s| - |V_{refi}|}{n_{qi}}}$ in order for $\dfrac{Q_{DGi}^{rated}}{\Delta |V_i^{\max}|} \dfrac{(|V_i^s| - |V_{refi}|)}{\sum_{i=1}^{N_{DG}} \dfrac{|V_i^s| - |V_{refi}|}{n_{qi}}}$ to balance the desired value of $\dfrac{Q_{DGi}^s}{\sum_{i=1}^{N_{DG}} Q_{DGi}^s}$.

In conclusion, in the scenario of appropriate active power allocation, to reach the tuning values of $m_{pi}$, we must compute the ideal active power sharing coefficient values. Furthermore, in the scenario of suitable reactive production power allocation, when the ideal values of the reactive power sharing coefficient are known. To obtain those values, the proper values of $n_{qi}$ and $|V_{refi}|$ must be tuned inside the predetermined ranges.

# CHAPTER

# 4

# OPTIMAL PLANNING OF DROOP-DG IN ISLANDED AC MICROGRID FOR LOST POWER MITIGATION AND BUS VOLTAGE IMPROVEMENT

In this chapter, metaheuristic based on DE and HB techniques, along with the MBFS load flow approach, are described in Chapter 3 and applied in order to detect the suitable allocation (that is, site and capacity) of droop-DGs within the IEEE 33-bus DIMG. This study aims to mitigate lost active and reactive power, as well as to boost the nodal voltage magnitude. The following presents the content of this chapter.

## 4.1 Mathematical modelling formulation

### 4.1.1 Fitness/Objective functions

The main focus is on minimising DIMG's lost active power $F_1$, while taking into account lost reactive power $F_2$, total node voltage variation $F_3$, and maximising nodal VSI $F_4$.

$$\min \ F_1(\boldsymbol{x}) \tag{4.1}$$

$$\boldsymbol{x} = [\boldsymbol{x_{loc}}, \boldsymbol{x_{m_p}}, \boldsymbol{x_{n_q}}, \boldsymbol{x_{Vref}}]$$

$$\boldsymbol{x_{loc}} = [loc_1,\ loc_2, ...,\ loc_i], \quad \boldsymbol{x_{m_p}} = [m_{p1},\ m_{p2}, ...,\ m_{pi}],$$

$$\boldsymbol{x_{n_q}} = [n_{q1},\ n_{q2}, ...,\ n_{qi}], \quad \boldsymbol{x_{V_{ref}}} = [|V_{ref1}|,\ |V_{ref2}|, ...,\ |V_{refi}|],$$

where: the vector $\boldsymbol{x}_{\boldsymbol{loc}}$ denotes location of all DGs, while the vectors $\boldsymbol{x}_{\boldsymbol{m_p}}$ and $\boldsymbol{x}_{\boldsymbol{n_q}}$ represent their $f$ and $V$ droop gains respectively; the vector $\boldsymbol{x}_{\boldsymbol{V_{ref}}}$ signifies DGs' reference voltage magnitude; $i \in [1, N_{DG}] \cap Z$, the DIMG number of DGs is denoted by $N_{DG}$ while $Z$ represents a numerical integer; $loc_i$ is site of the $i$-th droop-DG; $m_{pi}$ and $n_{qi}$ represent $f$ and $V$ droop gains of the $i$-th droop-DG respectively; $|V_{refi}|$ is reference voltage magnitude.

Fig. 4. 1 shows the branch structure in radial networks consisting of sending and receiving end node voltages $V_j$ and $V_{j+1}$, impedance between two nodes $Z_k$, the $k$-th branch's current flow $I_k$, and the production power provided through the $(j+1)$-th bus $P_{j+1}$ and $Q_{j+1}$.

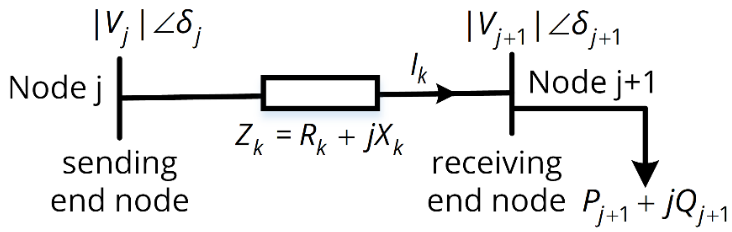


Fig. 4. 1 The structure of the radial branch

Power losses fall on the branches during the transfer process, which are considered as objective functions, and are determined by

$$F_1 = \sum_{t=1}^{T} \sum_{k=1}^{N_{br}} R_k I_k^2 \tag{4.2}$$

$$F_2 = \sum_{t=1}^{T} \sum_{k=1}^{N_{br}} X_k I_k^2 \tag{4.3}$$

where: $R_k$ and $X_k$ denote the $k$-th branch's resistance and reactance respectively; the DN's number of branches is represented by $N_{br}$; the entire investigated time is indicated by $T$.

The indicator of total nodal voltage deviation is used to verify the efficiency of the suggested methodologies for the proper allocation of droop-DGs in DIMG and given as

$$F_3 = \sum_{t=1}^{T}\sum_{j=1}^{N} |1 - V_j| \tag{4.4}$$

where: the DN's number of buses is denoted by $N$.

The VSI indicator is also proposed to detect nodes that are susceptible to voltage collapse [143]. A DIMG system that functions in a stable state if the value of VSI on each node is above zero [97]. Additionally, $VSI_{(j+1)}(t)$ has a large value, this contributes considerably to enhancing the stable DIMG operating, and is determined by

$$VSI_{(j+1)}(t) = |V_j|^4 - 4(P_{j+1}X_k - Q_{j+1}R_k)^2 - 4(P_{j+1}R_k + Q_{j+1}X_k)|V_j|^2 \tag{4.5}$$

$$F_4 = VSI_{(j+1)}(t) \tag{4.6}$$

where: $\forall j \in [1, N] \cap Z$, $\forall k \in [1, N-1] \cap Z$; $VSI_{(j+1)}(t)$ is the VSI of bus $(j+1)$ at the investigated time $t$.

### 4.1.2 Operational constraints in a DIMG

Under steady-state operating conditions, the power injection from all droop-DGs into load buses is expressed as in equations (4.7) and (4.8). These two equations are known as nonlinear load flow equations.

$$\begin{aligned}\sum_{i=1}^{N_{DG}} \frac{1}{m_{pi}}\left(f(t) - f_{ref}\right) + \sum_{i=1}^{N_{DG}} P_{DGio} - \sum_{i=1}^{N} P_{Li}(t) \\ = \sum_{i=1}^{N}\sum_{j=1}^{N} |V_i(t)||V_j(t)||Y_{ij}(t)|\cos\left(\delta_i(t) - \delta_j(t) - \theta_{ij}(t)\right)\end{aligned} \tag{4.7}$$

$$\begin{aligned}\sum_{i=1}^{N_{DG}} \frac{1}{n_{qi}}\left(|V_i(t)| - |V_{refi}(t)|\right) + \sum_{i=1}^{N_{DG}} Q_{DGio} - \sum_{i=1}^{N} Q_{Li}(t) \\ = \sum_{i=1}^{N}\sum_{j=1}^{N} |V_i(t)||V_j(t)||Y_{ij}(t)|\sin\left(\delta_i(t) - \delta_j(t) - \theta_{ij}(t)\right)\end{aligned} \tag{4.8}$$

where: $m_{pi}$ and $n_{qi}$ denote the $P$ and $Q$ droop gains of droop-DG $i$ at time $t$ respectively; $f(t)$ represents the operating frequency at time $t$; $f_{ref}$ is the DIMG's reference frequency; $P_{DGio}$ and $Q_{DGio}$ signify the reference powers of droop-DG $i$; $P_{Li}(t)$ represents the load's active power consumption at time $t$, while $Q_{Li}(t)$ denotes the reactive power consumption; $|V_{refi}(t)|$ is the magnitude of the reference voltage of droop-DG $i$ at time $t$; $V_i(t)$ and $V_j(t)$ denote the working voltage magnitudes of buses $i$ and $j$ at time $t$; $\delta_i(t)$ and $\delta_j(t)$ signify the phase angles of the working voltage of node $i$ and node $j$ at time $t$; the phase angle and magnitude of the branch admittance between two nodes $i$ and $j$ at time $t$ are expressed by $\theta_{ij}(t)$ and $|Y_{ij}(t)|$.

Constraints (4.9) and (4.10) are to keep the DIMG's voltage frequency and magnitude inside standard ranges [3]. To operate dispatchable DGs based on the droop law in a steady state, their output powers at any time should conform to constraints (4.11) and (4.12). These limits depend on the producer standard for each type of DG. Constraint (4.13) describes the tuned limit of each DG set voltage magnitude to decrease the nodal voltage variation from the reference value. Constraints (4.14) and (4.15), along with constraint (4.13) maintain the DG's output power at the desired value inside a permitted range to satisfy load requirements, decrease the deviation of the operating voltage and frequency of a DIMG, etc.

$$f^{\min} \leq f(t) \leq f^{\max}, \quad t \in [1, T] \cap Z \tag{4.9}$$

$$|V^{\min}| \leq |V_i(t)| \leq |V^{\max}|, \quad i \in [1, N] \cap Z \tag{4.10}$$

$$P_{DGi}^{\min} \leq P_{DGi}(t) \leq P_{DGi}^{\max}, \quad i \in [1, N_{DG}] \cap Z \tag{4.11}$$

$$Q_{DGi}^{\min} \leq Q_{DGi}(t) \leq Q_{DGi}^{\max}, \quad i \in [1, N_{DG}] \cap Z \tag{4.12}$$

$$|V_{ref}^{\min}| \leq |V_{refi}(t)| \leq |V_{ref}^{\max}|, \quad i \in [1, N_{DG}] \cap Z \tag{4.13}$$

$$m_{pi}^{\min} \leq m_{pi}(t) \leq m_{pi}^{\max}, \quad i \in [1, N_{DG}] \cap Z \tag{4.14}$$

$$n_{qi}^{\min} \leq n_{qi}(t) \leq n_{qi}^{\max}, \quad i \in [1, N_{DG}] \cap Z \tag{4.15}$$

The above constraints are used for the computation of an example illustrated in Section 4.2 below.

## 4.2 Case study

### 4.2.1 Investigated cases

In this chapter, DE and HB techniques, together with the MBFS power flow approach, are described in Chapter 3, which are applied to ascertain the right droop-DG place and size within a standard IEEE 33-bus IMG network [144]. This IMG network is a preferred choice for experiments as a reference to verify the efficacy of the proposed methodologies, facilitating comparisons and assessments of distinct approaches and algorithms in established work.

To assess the operability of the suggested methodologies in identifying the ideal allocation of droop-DGs within the previously mentioned IMG, in this work, four cases are selected for the experiment. These cases are representative of the impact of optimising both separate and combined decision variables to lower lost power and gain bus voltage and voltage stability margin.

**Case 1:** Optimise the droop coefficients (i.e., size including $m_{pi}$ and $n_{qi}$) of five droop-DGs, while each DG's reference voltage $|V_{refi}|$ is fixed at 1.0 pu

**Case 2:** Optimise the droop parameters (i.e., size including $m_{pi}$, $n_{qi}$, and $|V_{refi}|$) of five droop-DGs, where each DG's reference voltage $|V_{refi}|$ is tuned inside the predefined range of 1.0–1.2 pu

**Case 3:** Optimise the simultaneous droop coefficients and placement of five droop-DGs, while the reference voltage of each DG is fixed at 1.0 pu

**Case 4:** Optimise the simultaneous droop parameters and placement of five droop-DGs, where the reference voltage of each DG is tuned inside the predetermined range of 1.0–1.2 pu.

### 4.2.2 Data for the test system

The IEEE 33-bus DIMG grid [144] is experimented for the appropriate allocation of five droop-DGs using the methodologies proposed in Chapter 3. In this work, the number of droop-DGs is chosen to be five units, with the aim of evaluating and comparing the suggested methodologies with an existing method. The investigated system's rated electrical demands are 3715 kW and 2300 kvar, while the voltage magnitude is 12.66 kV when rated. The test system-related data are the following. Fig. 4. 2 shows the reconfigured IEEE 33-bus DIMG topology. Furthermore, Tables A. 1 and A. 2 in the Appendix section represent line and load parameters of the IMG test system mentioned above respectively. The droop-DGs are powered by gas turbines and fuel cells, and the electrical load is fulfilled by these types of generators.

In this work, constant power load modelling is used, and the load modelling values are described in detail as in Table 4. 1. The power reference points for all DGs in droop are given as in Table 4. 2.

In this study, the DE/rand/1/bin-based mutation strategy is used. The predefined settings of the DE and HB techniques are shown in Tables 4. 3 and 4. 4 respectively. The upper power thresholds of five droop-DGs are tabulated in Table 4. 5. The bottom and top thresholds of the DIMG working voltage frequency and magnitude, and each droop-DG reference voltage magnitude for this study, are presented in Table 4. 6. Furthermore, the ideal site of five droop-DGs in the 33-bus DIMG for Cases 1 and 2 is assumed as mentioned in [23] (that is, at the following nodes 1, 6, 13, 25, and 33). This work's investigated load is designated to a level of 40%, 60%, 80%, and 100% of the nominal capacity corresponding to the timespan $t \in [1,\ 4]$, as illustrated within Fig. 4. 3.

The top and bottom $P$ droop coefficients $m_{pi}^{\max}$ and $m_{pi}^{\min}$ are $1.06\frac{f^{\min} - f_{ref}}{P_{DGi}^{rated} - P_{DGio}}$ and $21\frac{f^{\min} - f_{ref}}{P_{DGi}^{rated} - P_{DGio}}$ respectively. The upper and lower $Q$ droop gains $n_{qi}^{\max}$ and $n_{qi}^{\min}$ are $1.07\frac{|V_{ref}^{\min}| - |V_{ref}^{\max}|}{Q_{DGi}^{rated} - Q_{DGio}}$ and $27\frac{|V_{ref}^{\min}| - |V_{ref}^{\max}|}{Q_{DGi}^{rated} - Q_{DGio}}$ respectively.

Table 4. 1 The given parameters of load modelling

| **Parameters** | **Values** |
|---|---|
| $p$ | 0 |
| $q$ | 0 |
| $K_{pf}$ | 0 |
| $K_{qf}$ | 0 |

Table 4. 2 Power set points for five DGs

| **Parameters** | **Values** (pu) |
|---|---|
| $P_{DGio}$ | 0.2 |
| $Q_{DGio}$ | 0.2 |

Table 4. 3 Pre-determined settings for the DE algorithm

| **Cases** | $G_{\max}$ | $S_D$ | $F$ | $CR$ | $D_D$ |
|---|---|---|---|---|---|
| 1 | 20 | 30 | 0.2 | 0.5 | 10 |
| 2 | 20 | 30 | 0.2 | 0.5 | 15 |
| 3 | 15 | 20 | 0.2 | 0.5 | 15 |
| 4 | 15 | 20 | 0.2 | 0.5 | 20 |

Table 4. 4 Predetermined settings for the HB algorithm

| **Cases** | $IT_{\max}$ | $S_H$ | β | $C$ | $D_H$ |
|---|---|---|---|---|---|
| 1 | 20 | 30 | 6 | 2 | 10 |
| 2 | 20 | 30 | 6 | 2 | 15 |
| 3 | 15 | 20 | 6 | 2 | 15 |
| 4 | 15 | 20 | 6 | 2 | 20 |

Table 4. 5 Upper power thresholds of five DGs

| **DDG no.** | DDG1 | DDG2 | DDG3 | DDG4 | DDG5 |
|---|---|---|---|---|---|
| $P_{DDGi}^{\max}$ (kW) | 950 | 875 | 800 | 775 | 700 |
| $Q_{DDGi}^{\max}$ (kvar) | 520 | 515 | 510 | 505 | 490 |

Table 4. 6 Lower and upper thresholds of the IMG operating frequency and voltage, and DG's reference voltage magnitude

| $f^{\min}$ (pu) | $f^{\max}$ (pu) | $\lvert V^{\min}\rvert$ (pu) | $\lvert V^{\max}\rvert$ (pu) | $\lvert V_{ref}^{\min}\rvert$ (pu) | $\lvert V_{ref}^{\max}\rvert$ (pu) |
|---|---|---|---|---|---|
| 0.99 | 1.0 | 0.95 | 1.05 | 1.0 | 1.02 |

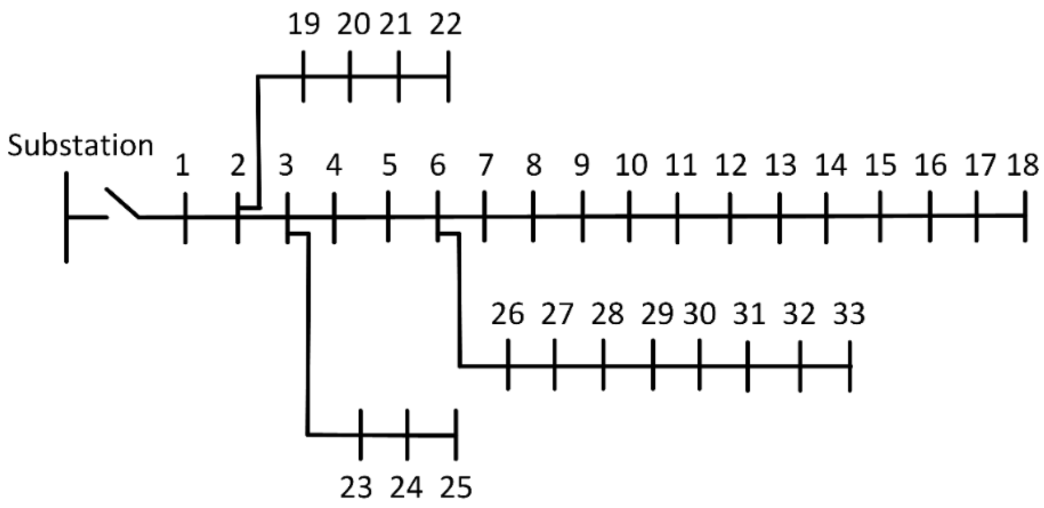


Fig. 4. 2 The reconfigured IEEE 33-bus DIMG topology

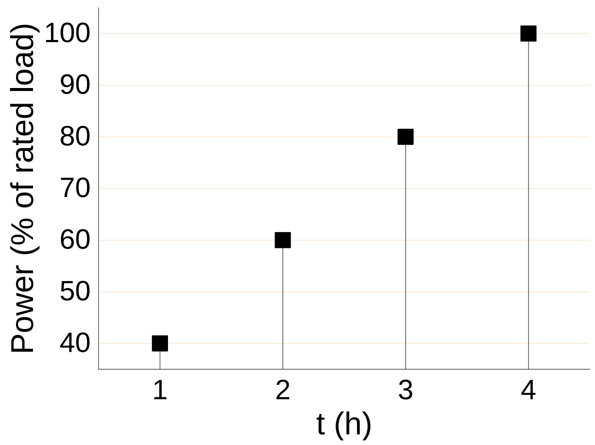


Fig. 4. 3 Investigated load profile t (h)

### 4.3 Results and discussion

As mentioned in Section 4.1.1, in order to optimise the control variables, the experiment was run on a computer. The machine was used to independently run each case 40 times, using the suggested parameters for both the DE and HB techniques, to guarantee the accuracy of the results.

The following shows the results achieved after simulating the proposed problem in the MATLAB tool. These outcomes are published in [129].

Tables 4. 7 and 4. 9 tabulate the tuned values of five DGs' reference voltage magnitude for Cases 2 and 4, while Figs. 4. 4 and 4. 5 list their optimal droop gains for Cases 1–4 in the load profile as referred to in Fig. 4. 3 through both DE and HB techniques. These droop parameters (i.e., $m_{pi}$, $n_{qi}$, and $|V_{refi}|$) optimise the five DGs' production power for the levels of the previously mentioned load profile. The information from Figs. 4. 4 and 4. 5 reveals that the power yield by five DGs increased with increasing values of the droop gains $m_p$ and $n_q$. In contrast, their generated powers decreased with decreasing levels of $m_p$ and $n_q$. The tuning of DGs' droop parameters is to meet the load and minimise power mismatches.

For Cases 3 and 4, Table 4. 8 shows where five droop-DGs should be placed on the 33-bus DIMG based on their respective DE and HB algorithms' sites. As indicated by the data in Tables 4. 13 and 4. 14, the inclusion of decision variables to identify the best placements for droop-DG leads to a more significant mitigation of losses in Cases 3 and 4 as opposed to Cases 1 and 2. Furthermore, the concurrent tuning of the DG droop parameters, together with optimal site in Case 4, effectively minimises power losses compared to the remaining cases, as depicted in Tables 4. 13 and 4. 14. This approach also helps reduce the total voltage deviation. In addition, it improves the nodal voltage and voltage stability index of the 33-bus DIMG, as presented within Figs. 4. 6 and 4. 7 respectively.

The operating frequency on the 33-bus DIMG for four investigated cases relating to the aforementioned load profile, which is computed through two metaheuristic algorithms, is shown in Table 4. 10. Each frequency value in this table complies with the mentioned constraints. In the meantime, the rated powers yielded by five droop-DGs between cases using each algorithm are presented in Tables 4. 11 and 4. 12. These optimal values based on control variables are tuned including variables such as droop parameters and site.

Table 4. 13 tabulates the objective functions and the percentage of losses for four cases using two DE and HB techniques. One of the potential benefits of functioning the microgrid electric system in islanded mode is to lower the lost power; Active power loss percentages between 0.5% and 1.5% of the rated load are allowed [94]. Data from Table 4. 13 point out that the best (lowest) power losses relate to

Case 4 using the HB algorithm with 19.2 kW and 17.45 kvar. Additionally, Case 4 using the HB approach yields the best (lowest) percentages of lost reactive and real power, at 0.271% and 0.184% respectively. On the other hand, the application of the DE technique in Case 1 produces the worst (highest) numerical results for power losses and percentages of loss. This table demonstrates that losses are considerably reduced when the HB algorithm is applied to the proposed model. Furthermore, Case 2 produces the better value in order to decrease the overall voltage deviation using the HB method, but Cases 1 and 3 give the worse values for both algorithms.

In this work, the experimental results at the rated power load level are compared with the numerical results shown in Table 4 [23], playing the role of a base case. In this table, the corresponding lost active and reactive powers are 17.2 kW and 13.0 kvar. In contrast to the base case, lost power in lines is greatly minimised in Cases 1–4 using the DE algorithm and the HB algorithm, as displayed in Table 4. 14. Furthermore, with the HB approach, Case 4 produces the best losses and the percentage of lost active and reactive power minimisation, while Case 1 utilising the DE and HB techniques yields the worst findings. Also, when comparing Cases 2 and 4 with Cases 1 and 3, and the base case, the total voltage deviation shows lower values.

Figs. 4. 6 and 4. 7 show the nodal voltage magnitude and the bus VSI of the DIMG test system at the nominal power load level for the respective cases utilising the DE algorithm and the HB algorithm. The information in these figures reveals that the optimal node voltage and VSI at all IMG nodes are found in Case 4, which uses the HB technique. On the other hand, Case 1's DE technique produces the worst outcomes. The figures above illustrate how the nodal voltage and VSI can be increased using the best DG droop parameters and location.

As indicated in Table 4. 15, when utilising the DE technique, the minimal nodal voltage magnitude values for Cases 2 and 4 are greater than those for Cases 1 and 3 when using the HB approach. Furthermore, using the DE technique, the optimal VSI value is found for Case 4, and the worst value is identified for Case 1.

Table 4. 7 $|V_{ref}|$ (pu) reference voltage values of five droop-DGs in Case 2

| **Methods** | **DDG no.** | **Percentage of nominal power load** | | | |
|---|---|---|---|---|---|
| | | **40%** | **60%** | **80%** | **100%** |
| DE | DDG1 | 1.0109 | 1.0139 | 1.0112 | 1.0156 |
| | DDG2 | 1.0190 | 1.0127 | 1.0188 | 1.0146 |
| | DDG3 | 1.0117 | 1.0128 | 1.0064 | 1.0118 |
| | DDG4 | 1.0113 | 1.0158 | 1.0083 | 1.0160 |
| | DDG5 | 1.0182 | 1.0199 | 1.0195 | 1.0143 |
| HB | DDG1 | 1.0105 | 1.0124 | 1.0156 | 1.0137 |
| | DDG2 | 1.0200 | 1.0200 | 1.0200 | 1.0166 |
| | DDG3 | 1.0000 | 1.0143 | 1.0080 | 1.0143 |
| | DDG4 | 1.0005 | 1.0147 | 1.0066 | 1.0167 |
| | DDG5 | 1.0200 | 1.0200 | 1.0200 | 1.0168 |

Table 4. 8 The proper site (node) of five droop-DGs in Cases 3 and 4

| **Cases** | **Methods** | **DDG1** (node) | **DDG2** (node) | **DDG3** (node) | **DDG4** (node) | **DDG5** (node) |
|---|---|---|---|---|---|---|
| 3 | DE | 30 | 3 | 14 | 25 | 26 |
| | HB | 24 | 26 | 31 | 14 | 2 |
| 4 | DE | 24 | 26 | 31 | 2 | 13 |
| | HB | 30 | 19 | 25 | 6 | 14 |

Table 4. 9 $|V_{ref}|$ (pu) reference voltage values of five droop-DGs in Case 4

| Methods | DDG no. | Percentage of nominal power load | | | |
|---|---|---|---|---|---|
| | | 40% | 60% | 80% | 100% |
| DE | DDG1 | 1.0167 | 1.0100 | 1.0182 | 1.0151 |
| | DDG2 | 1.0178 | 1.0179 | 1.0199 | 1.0158 |
| | DDG3 | 1.0200 | 1.0190 | 1.0185 | 1.0133 |
| | DDG4 | 1.0188 | 1.0122 | 1.0086 | 1.0106 |
| | DDG5 | 1.0142 | 1.0027 | 1.0049 | 1.0108 |
| HB | DDG1 | 1.0188 | 1.0200 | 1.0200 | 1.0151 |
| | DDG2 | 1.0182 | 1.0000 | 1.0000 | 1.0167 |
| | DDG3 | 1.0057 | 1.0000 | 1.0128 | 1.0171 |
| | DDG4 | 1.0186 | 1.0048 | 1.0200 | 1.0177 |
| | DDG5 | 1.0136 | 1.0000 | 1.0000 | 1.0123 |

Table 4. 10 Values of the 33-bus DIMG frequency (pu) for four cases

| Cases | Methods | Percentage of nominal power load | | | |
|---|---|---|---|---|---|
| | | 40% | 60% | 80% | 100% |
| 1 | DE | 0.9903 | 0.9903 | 0.9901 | 0.9900 |
| | HB | 0.9900 | 0.9900 | 0.9900 | 0.9903 |
| 2 | DE | 0.9907 | 0.9900 | 0.9903 | 0.9901 |
| | HB | 0.9902 | 0.9901 | 0.9900 | 0.9900 |
| 3 | DE | 0.9904 | 0.9900 | 0.9900 | 0.9900 |
| | HB | 0.9901 | 0.9900 | 0.9902 | 0.9900 |
| 4 | DE | 0.9905 | 0.9901 | 0.9901 | 0.9900 |
| | HB | 0.9900 | 0.9910 | 0.9902 | 0.9900 |
| Base | – | – | – | – | 0.9984 |

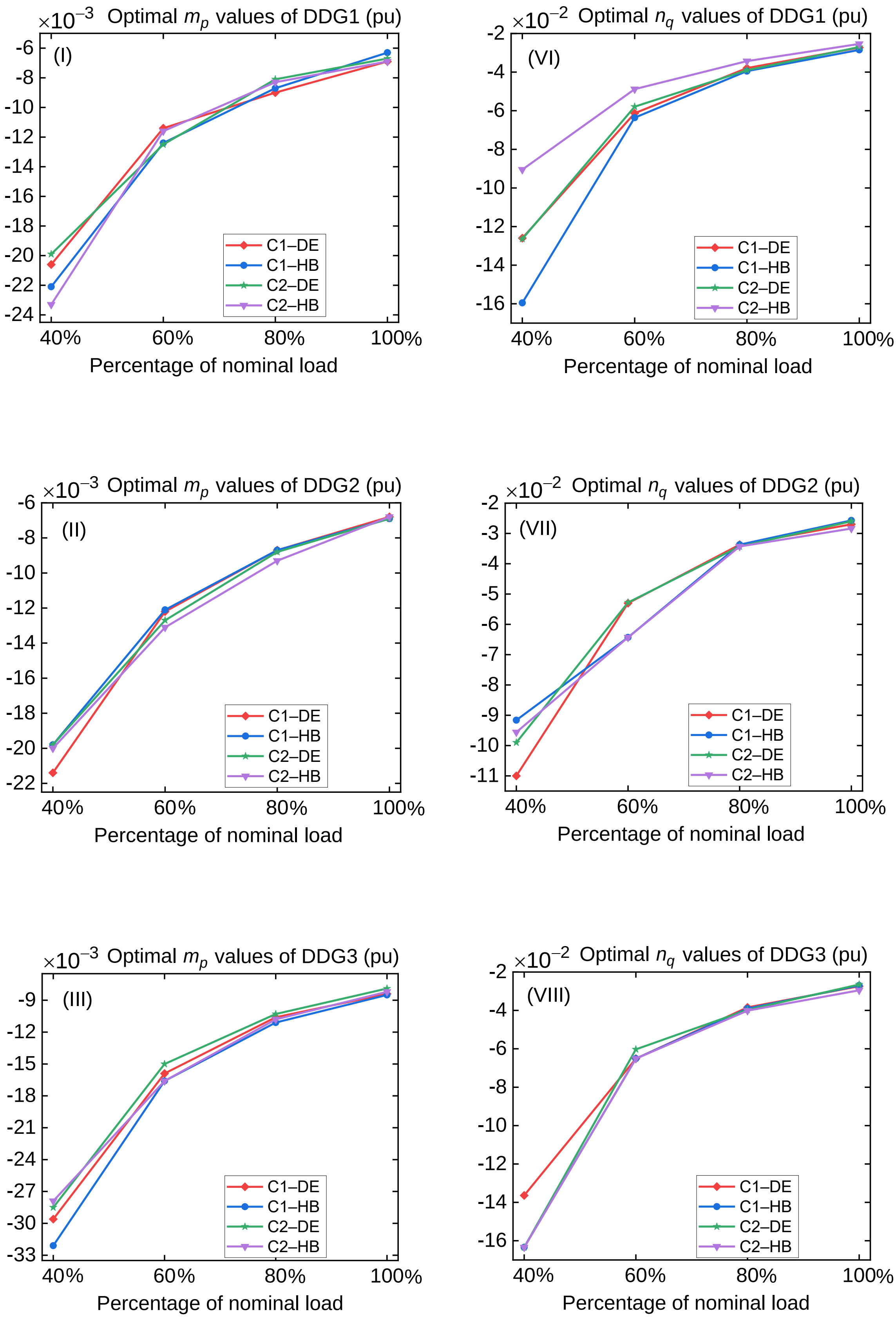


(Figures to be continued on the next page)

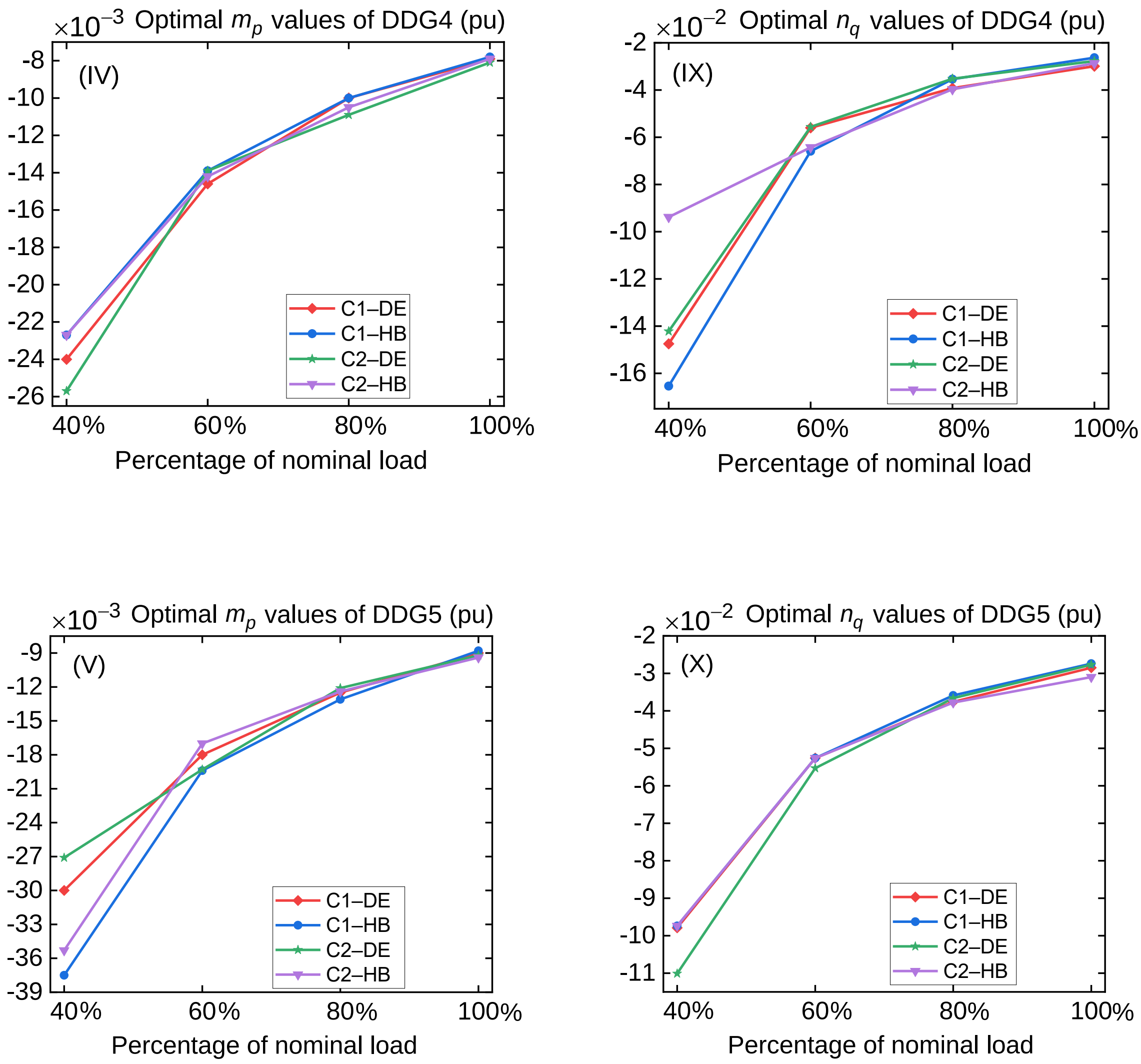


Fig. 4. 4 Optimal droop coefficients of five DGs 1–5 (categorised as I–V) concerning $m_p$ and droop gains of five DGs 1–5 (identified as VI–X) regarding $n_q$ for Cases 1 and 2

where: $Ci$ is the $i$-th Case with $i \in [1, 4]$.

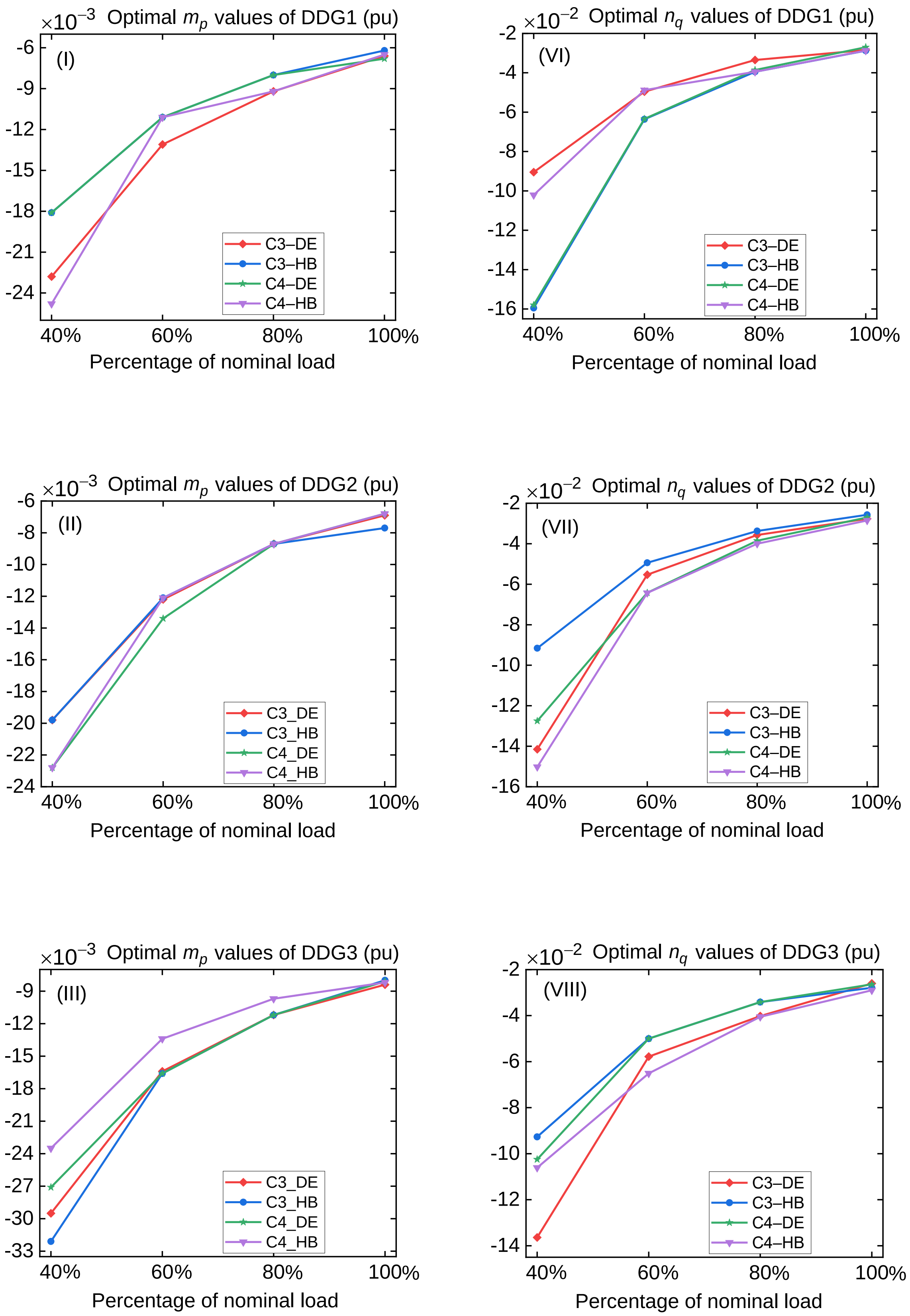


(Figures to be continued on the next page)

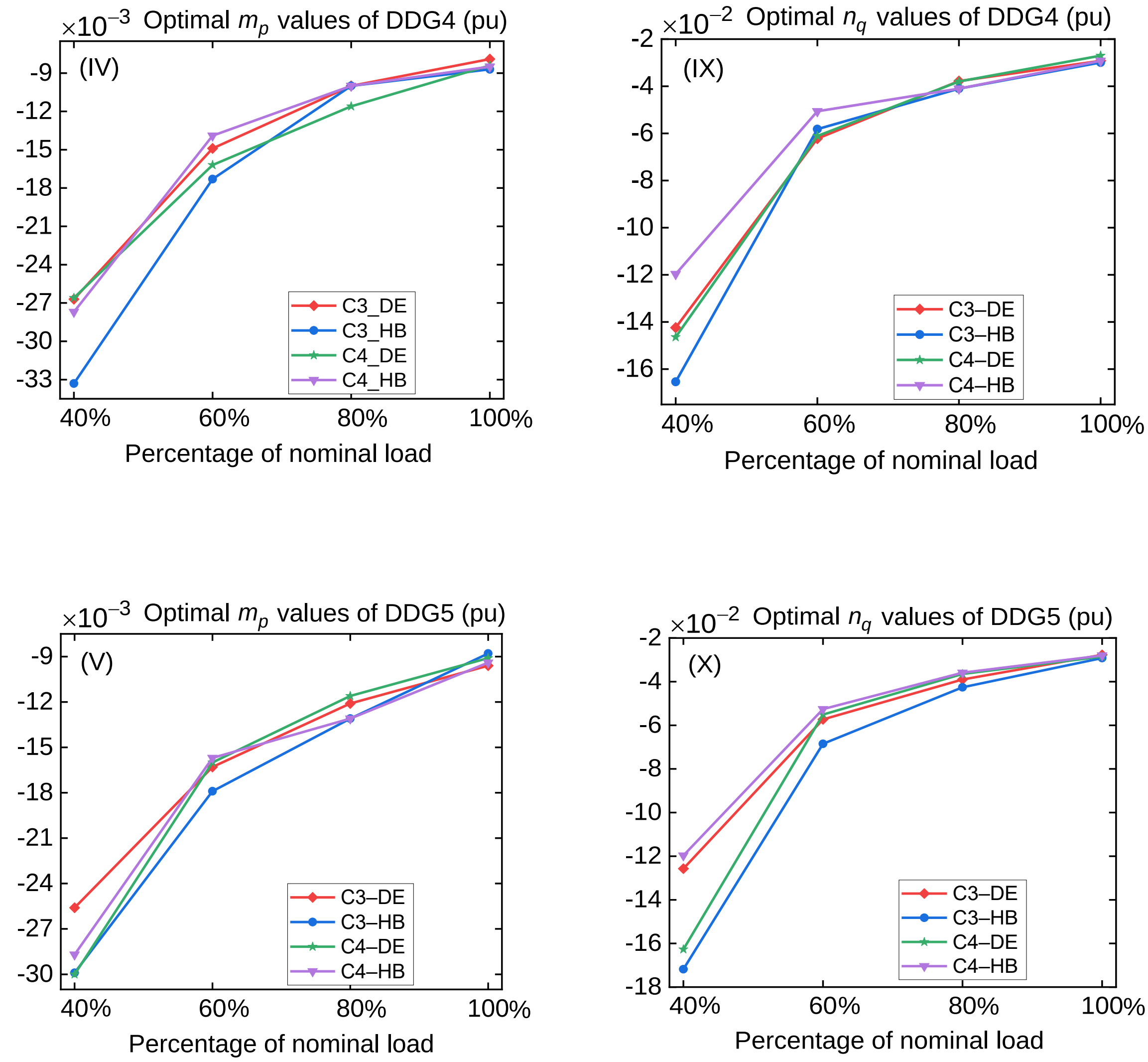


Fig. 4. 5 Optimal droop coefficients of five DGs 1–5 (categorised as I–V) concerning $m_p$ and droop gains of five DGs 1–5 (identified as VI–X) regarding $n_q$ for Cases 3 and 4

where: $Ci$ denotes the $i$-th Case with $i \in [1, 4]$.

Table 4. 11 The rated active power values (kW) of five droop-DGs for the cases

| Cases | Methods | DDG no. | | | | |
|---|---|---|---|---|---|---|
| | | DDG1 | DDG2 | DDG3 | DDG4 | DDG5 |
| 1 | DE | 821.20 | 829.65 | 694.75 | 728.60 | 653.75 |
| | HB | 872.00 | 806.80 | 672.40 | 723.80 | 652.90 |
| 2 | DE | 838.05 | 817.00 | 725.45 | 709.85 | 637.25 |
| | HB | 821.90 | 831.70 | 711.70 | 729.80 | 632.45 |
| 3 | DE | 859.50 | 822.25 | 695.70 | 730.30 | 618.15 |
| | HB | 906.30 | 749.35 | 727.05 | 674.20 | 668.20 |
| 4 | DE | 833.60 | 833.60 | 715.85 | 693.85 | 648.20 |
| | HB | 866.20 | 830.30 | 711.45 | 684.20 | 632.85 |
| Base | – | 800.30 | 800.30 | 800.30 | 800.30 | 533.55 |

Table 4. 12 The rated reactive power values (kvar) of five droop-DGs in the cases

| Cases | Methods | DDG no. | | | | |
|---|---|---|---|---|---|---|
| | | DDG1 | DDG2 | DDG3 | DDG4 | DDG5 |
| 1 | DE | 461.25 | 507.65 | 416.75 | 436.95 | 488.15 |
| | HB | 425.20 | 514.30 | 419.30 | 459.35 | 490.00 |
| 2 | DE | 466.45 | 511.40 | 367.85 | 470.40 | 489.75 |
| | HB | 454.20 | 510.10 | 382.70 | 467.10 | 489.85 |
| 3 | DE | 519.45 | 482.00 | 394.25 | 433.10 | 475.50 |
| | HB | 460.55 | 510.05 | 508.25 | 380.40 | 448.20 |
| 4 | DE | 504.85 | 507.65 | 505.95 | 407.20 | 374.60 |
| | HB | 520.00 | 450.55 | 462.35 | 502.25 | 365.75 |
| Base | – | 1180.50 | 187.60 | 166.20 | 155.20 | 626.70 |

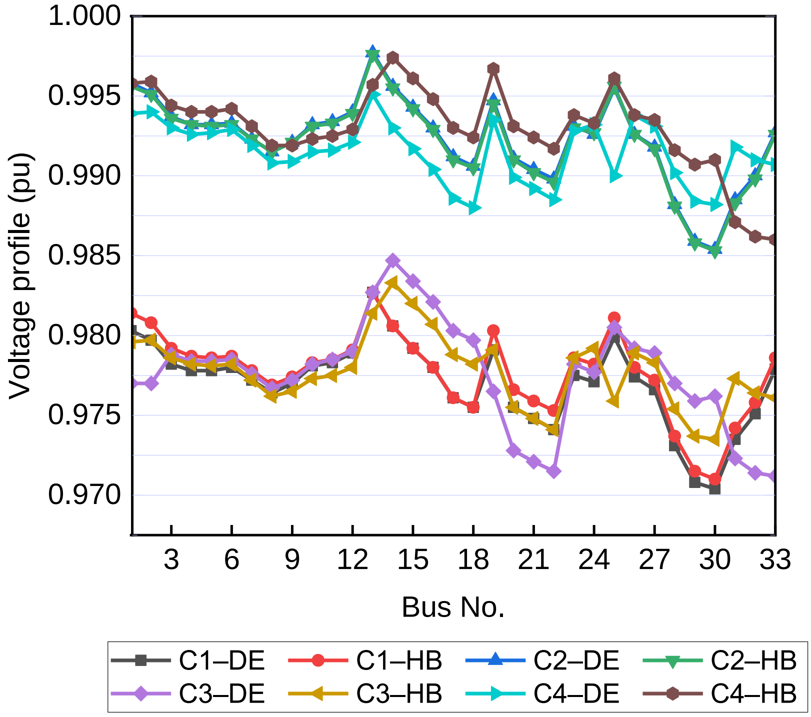


Fig. 4. 6 Voltage profile (pu) of the investigated DIMG at the nominal load

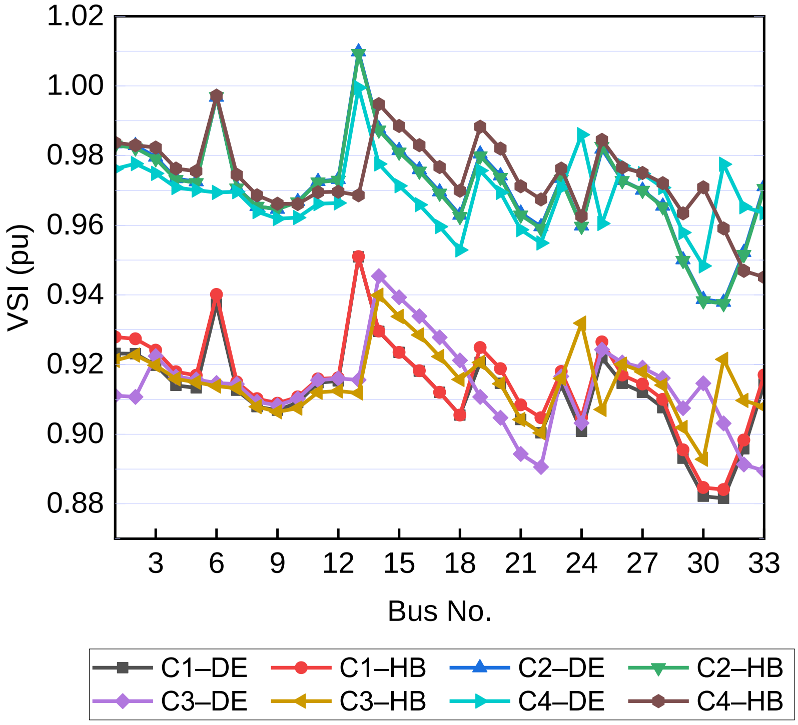


Fig. 4. 7 Voltage stability index (pu) of the investigated DIMG at the nominal load

where: $Ci$ is the $i$-th Case with $i \in [1, 4]$.

Table 4. 13 Comparison of objective functions, percentage of lost active power (percentage of $P_{loss}$), and percentage of lost reactive power (percentage of $Q_{loss}$) for cases

| **Objectives** | **Methods** | **Cases** | | | |
|---|---|---|---|---|---|
| | | **1** | **2** | **3** | **4** |
| $F_1$ (kW) | DE | 27.55 | 26.10 | 22.70 | 20.50 |
| | **HB** | 27.40 | 25.90 | 21.60 | **19.20** |
| $F_2$ (kvar) | DE | 25.55 | 24.50 | 19.75 | 18.65 |
| | **HB** | 25.40 | 24.35 | 19.15 | **17.45** |
| $F_3$ (pu) | DE | 2.915 | 1.001 | 2.865 | 1.034 |
| | HB | 2.966 | 0.961 | 2.858 | 1.328 |
| Percentage of $P_{loss}$ (%) | DE | 0.265 | 0.251 | 0.218 | 0.197 |
| | **HB** | 0.263 | 0.249 | 0.208 | **0.184** |
| Percentage of $Q_{loss}$ (%) | DE | 0.396 | 0.380 | 0.306 | 0.290 |
| | **HB** | 0.395 | 0.378 | 0.297 | **0.271** |

Table 4. 14 Comparison of power losses $P_{loss}$ and $Q_{loss}$, percentage of lost active power minimisation (% $P_{loss}$ minimisation) and lost reactive power minimisation (% $Q_{loss}$ minimisation), and sum nodal voltage variation ΔV at the nominal load

| **Cases** | **Methods** | $P_{loss}$ (kW) | % $P_{loss}$ minimisation | $Q_{loss}$ (kvar) | % $Q_{loss}$ minimisation | $\Delta V$ (pu) |
|---|---|---|---|---|---|---|
| Base | – | 17.20 | – | 13.00 | – | 0.634 |
| 1 | DE | 12.90 | 25.00 | 11.95 | 8.08 | 0.758 |
| | HB | 12.90 | 25.00 | 11.95 | 8.08 | 0.737 |
| 2 | DE | 12.60 | 26.74 | 11.55 | 11.15 | 0.255 |
| | HB | 12.45 | 27.62 | 11.50 | 11.54 | 0.257 |
| 3 | DE | 10.90 | 36.63 | 9.40 | 27.69 | 0.740 |
| | HB | 10.05 | 41.57 | 8.90 | 31.54 | 0.727 |
| **4** | DE | 10.10 | 41.28 | 9.05 | 30.38 | 0.281 |
| | **HB** | **10.00** | **41.86** | **8.90** | **31.54** | **0.231** |

Table 4. 15 Minimal working voltage magnitude and VSI in (pu) of the investigated DIMG at the nominal load

| **Cases** | **Methods** | $\lvert V_i \rvert$ (bus) | VSI (bus) |
|---|---|---|---|
| 1 | DE | 0.9704 (30) | 0.8816 (31) |
| | HB | 0.9710 (30) | 0.8841 (31) |
| 2 | DE | 0.9854 (30) | 0.9379 (31) |
| | HB | 0.9853 (30) | 0.9375 (31) |
| 3 | DE | 0.9712 (33) | 0.8895 (33) |
| | HB | 0.9735 (30) | 0.8928 (30) |
| 4 | DE | 0.9880 (18) | 0.9483 (30) |
| | HB | 0.9860 (33) | 0.9451 (33) |
| Base | – | 0.9733 (30) | – |

## 4.4 Conclusion

In this work, the proper droop-DG positioning and sizing in the islanded microgrid are achieved in order to minimise lost power in lines and enhance the bus voltage, considering load demand variations over time. From the above-mentioned analyses and discussion, the HB algorithm is demonstrated to be an efficient technique for tackling the ideal allocation (i.e., site and size) of five droop-DGs within the DIMG to mitigate lost power and gain bus voltage magnitude (as illustrated in Case 4, Tables

4. 13 and 4. 14). Furthermore, when simultaneous tuning of the DG droop parameters and site helps the DIMG system considerably minimise lost active and reactive power, as well as improve nodal voltage.

# CHAPTER

# 5

# MULTIPLE DROOP–DG SITES IN AN ISLANDED AC MICROGRID FOR LOST POWER MITIGATION AND BUS VOLTAGE IMPROVEMENT

An effective method to minimise the degree of lost powers in distribution grids is the deployment of a suitable number of DGs. To implement this approach, small-sized DGs can be installed on the grid. This not only helps in minimising potential losses but also enhances the efficient use of the distribution network, such as maintaining a stable voltage, improving power quality, etc. This chapter is conducted as follows.

## 5.1 Mathematical modelling formulation

### 5.1.1 Objective functions

In this work, lost active power $F_a$ is taken into account as an objective function in order to optimise it to the minimum value, while mitigating lost reactive power $F_b$. The optimisation of these objective functions based on decision variables is described as

$$\min F_a(\boldsymbol{x}) \tag{5.1}$$

$$\boldsymbol{x} = [\boldsymbol{x_{pos}}, \boldsymbol{x_{capa}}, \boldsymbol{x_{Vref}}]$$

$$\boldsymbol{x_{pos}} = [pos_1, pos_2, \ldots, pos_i], \quad \boldsymbol{x_{capa}} = [m_{p1}, m_{p2}, \ldots, m_{pi}, n_{q1}, n_{q2}, \ldots, n_{qi}],$$

$$\boldsymbol{x}_{\boldsymbol{V_{ref}}} = [|V_{ref1}|, |V_{ref2}|, \ldots, |V_{refi}|],$$

where: the vector $\boldsymbol{x}_{\boldsymbol{pos}}$ denotes location of all DGs, while the vector $\boldsymbol{x}_{\boldsymbol{capa}}$ signifies their $f$ and $V$ droop gains; the vector $\boldsymbol{x}_{\boldsymbol{V_{ref}}}$ is DGs' reference voltage magnitude; $i \in [1, N_{DG}] \cap Z$, the number of droop-DGs functioning in the power grid to meet load demands is denoted by $N_{DG}$ while $Z$ represents a numerical integer; $pos_i$ is site of the $i$-th droop-DG; $m_{pi}$ and $n_{qi}$ represent $f$ and $V$ droop gains of the $i$-th droop-DG respectively; $|V_{refi}|$ is reference voltage magnitude.

Power losses on the radial branches of a DIMG as depicted in Fig. 4. 1, Chapter 4 can be determined by,

$$F_a = \sum_{s=1}^{S}\sum_{k=1}^{N_{br}} R_k I_k^2 \tag{5.2}$$

$$F_b = \sum_{s=1}^{S}\sum_{k=1}^{N_{br}} X_k I_k^2 \tag{5.3}$$

where: in branch $k$, $R_k$ is the resistance, and $X_k$ expresses the reactance, while $I_k$ denotes the current through this branch; the DIMG number of branches is denoted by $N_{br}$; the investigated load scenarios are represented by $S$.

### 5.1.2 Operational constraints in a DIMG

Equations (5.4) and (5.5) are nonlinear load flow equations that describe the production power of droop-DG units injected into load buses, considering steady-state operating conditions.

$$\begin{aligned} &\sum_{i=1}^{N_{DG}} \frac{1}{m_{pi}}\left(f^s - f_{ref}\right) + \sum_{i=1}^{N_{DG}} P_{DGio} - \sum_{i=1}^{N} P_{Li}^s \\ &= \sum_{i=1}^{N}\sum_{j=1}^{N} |V_i^s||V_j^s||Y_{ij}^s|\cos\left(\delta_i^s - \delta_j^s - \theta_{ij}^s\right) \end{aligned} \tag{5.4}$$

$$\sum_{i=1}^{N_{DG}} \frac{1}{n_{qi}}\left(|V_i^s|-|V_{refi}^s|\right) + \sum_{i=1}^{N_{DG}} Q_{DGio} - \sum_{i=1}^{N} Q_{Li}^s = \sum_{i=1}^{N}\sum_{j=1}^{N} |V_i^s||V_j^s||Y_{ij}^s| \sin\left(\delta_i^s - \delta_j^s - \theta_{ij}^s\right) \tag{5.5}$$

where: $m_{pi}$ and $n_{qi}$ denote the $f$ and $V$ droop gains of the $i$-th droop-DG in scenario $s$ respectively; $f^s$ represents the operating frequency in scenario $s$; $f_{ref}$ denotes the DIMG's reference frequency; $P_{DGio}$ and $Q_{DGio}$ signify the reference powers of droop-DG $i$; $P_{Li}^s$ and $Q_{Li}^s$ express the load's power consumption in scenario $s$; $|V_{refi}^s|$ is the reference voltage of droop-DG $i$ in scenario $s$; $|V_i^s|$ and $|V_j^s|$ denote the working voltage of nodes $i$ and $j$ in scenario $s$; $\delta_i^s$ and $\delta_j^s$ signify the phase angles of the working voltage of bus $i$ and bus $j$ in scenario $s$; the line admittance phase angle and magnitude between two nodes $i$ and $j$ in scenario $s$ are denoted by $\theta_{ij}^s$ and $|Y_{ij}^s|$; $N$ denotes the DIMG number of nodes/buses.

The purpose of constraints (5.6) and (5.7) is to maintain the DIMG voltage magnitude and frequency inside standard ranges [3]. In an operational steady state, the production power of dispatchable droop-DGs is restricted by constraints (5.8) and (5.9). Where both upper and lower generation levels of DG are dependent on the producer standard. Constraint (5.10) expresses the tuned limit of the droop-DG reference voltage magnitude to minimise the node voltage deviation from the reference value. Constraints (5.10), (5.11), and (5.12) keep the production power of droop-DGs at the optimal value inside an allowed range to fulfil the demands of the electric load and reduce DIMG's voltage and frequency deviation.

$$f^{\min} \le f^s \le f^{\max}, \quad s \in [1, S] \cap Z \tag{5.6}$$

$$|V^{\min}| \le |V_i^s| \le |V^{\max}|, \quad i \in [1, N] \cap Z \tag{5.7}$$

$$P_{DGi}^{\min} \le P_{DGi}^s \le P_{DGi}^{\max}, \quad i \in [1, N_{DG}] \cap Z \tag{5.8}$$

$$Q_{DGi}^{\min} \leq Q_{DGi}^{s} \leq Q_{DGi}^{\max}, \quad i \in [1, N_{DG}] \cap Z \tag{5.9}$$

$$|V_{ref}^{\min}| \leq |V_{refi}^{s}| \leq |V_{ref}^{\max}|, \quad i \in [1, N_{DG}] \cap Z \tag{5.10}$$

$$m_{pi}^{\min} \leq m_{pi}^{s} \leq m_{pi}^{\max}, \quad i \in [1, N_{DG}] \cap Z \tag{5.11}$$

$$n_{qi}^{\min} \leq n_{qi}^{s} \leq n_{qi}^{\max}, \quad i \in [1, N_{DG}] \cap Z \tag{5.12}$$

The aforesaid constraints are employed for the computation of an example illustrated in Section 5.2 below.

## 5.2 Case study

### 5.2.1 Investigated cases

In this work, the DE algorithm and the MBFS power flow approach are introduced in Chapter 3, which are used in order to optimise the deployment of multiple droop-DG placements within the IEEE 33-bus DIMG grid [144].

To check the working capability of the suggested techniques for the suitable deployment of multiple droop-DG sites within the reconfigured 33-bus DIMG grid, four cases are selected below.

**Case 1:** Optimise the capacity of three DGs

**Case 2:** Optimise the simultaneous capacity and positioning of three DGs

**Case 3:** Optimise the capacity of five DGs

**Case 4:** Optimise the simultaneous capacity and positioning of five DGs.

In this study, five droop-DGs are used in order to assess and contrast the proposed approaches with existing techniques because the permitted computational resources are restricted. To maximise the extent of lost power mitigation, a number of DG units installing on the grid shall be greater than thirty percent of all IMG buses.

### 5.2.2 Data for the testing system

The investigated grid is the configured 33-bus DIMG as illustrated in Fig. 4. 2 of Chapter 4, which is employed for the proposed model. This system consisting of the nominal load is 3715 kW and 2300 kvar, while the voltage magnitude is 12.66 kV when rated. The branch and electrical load parameters of the grid are predetermined as in Tables A. 1 and A. 2 in the Appendix section. The 33-bus DIMG's energy needs are met by diesel generators and gas turbines, and 20% of these DGs' rated capacities is the minimum capacity these generators must have in order to provide the electric load.

The constant power load modelling is proposed in order to employ, and its parameters are determined in Table 5. 1. Also, Table 5. 2 shows the power reference points of the droop-DGs for all cases.

In this work, the strategy for mutation of the DE approach is based on DE/rand/1/bin. The predetermined parameters of the DE technique are set as in Table 5. 3. The upper power limits of the droop-DGs for cases are shown in Table 5. 4. The bottom and top thresholds of the working voltage frequency and magnitude, and the set voltage magnitude of each droop-DG for cases, are determined as in Table 5. 5. Regarding the positioning of the DG for Cases 1 and 3, it is assumed that it would be the same as in [46], that is, on buses 2, 12, and 26, and in [23], on buses 1, 6, 13, 25, and 33. For the two scenarios in the load profile study, the load demand is set at 30% and 100% levels of the nominal capacity at $s$ = 1 and $s$ = 2 respectively, as represented in Fig. 5. 1.

For three droop-DGs: The upper and lower $P$ droop coefficients $m_{pi}^{\max}$ and $m_{pi}^{\min}$ are $1.06\frac{f^{\min} - f_{ref}}{P_{DGi}^{rated} - P_{DGio}}$ and $18\frac{f^{\min} - f_{ref}}{P_{DGi}^{rated} - P_{DGio}}$ respectively. The upper and lower $Q$ droop gains $n_{qi}^{\max}$ and $n_{qi}^{\min}$ are $1.05\frac{|V_{ref}^{\min}| - |V_{ref}^{\max}|}{Q_{DGi}^{rated} - Q_{DGio}}$ and $30\frac{|V_{ref}^{\min}| - |V_{ref}^{\max}|}{Q_{DGi}^{rated} - Q_{DGio}}$ respectively.

For five droop-DGs: The upper and lower $P$ droop coefficients $m_{pi}^{\max}$ and $m_{pi}^{\min}$ are $1.06\frac{f^{\min} - f_{ref}}{P_{DGi}^{rated} - P_{DGio}}$ and $21\frac{f^{\min} - f_{ref}}{P_{DGi}^{rated} - P_{DGio}}$ respectively. The upper and lower $Q$ droop gains $n_{qi}^{\max}$ and $n_{qi}^{\min}$ are $1.07\frac{|V_{ref}^{\min}| - |V_{ref}^{\max}|}{Q_{DGi}^{rated} - Q_{DGio}}$ and $27\frac{|V_{ref}^{\min}| - |V_{ref}^{\max}|}{Q_{DGi}^{rated} - Q_{DGio}}$ respectively.

Table 5. 1 The parameters of the load modelling

| **Parameters** | **Values** |
|---|---|
| $p$ | 0 |
| $q$ | 0 |
| $K_{pf}$ | 0 |
| $K_{qf}$ | 0 |

Table 5. 2 The power set points of the DGs for all cases

| **Parameters** | **Values** (pu) |
|---|---|
| $P_{DGio}$ | 0.2 |
| $Q_{DGio}$ | 0.2 |

Table 5. 3 Pre-determined settings for the DE algorithm

| **Cases** | $G_{\max}$ | $S_D$ | $F$ | $CR$ | $D_D$ |
|---|---|---|---|---|---|
| 1 | 30 | 40 | 0.2 | 0.5 | 9 |
| 2 | 30 | 40 | 0.2 | 0.5 | 12 |
| 3 | 15 | 20 | 0.2 | 0.5 | 15 |
| 4 | 15 | 20 | 0.2 | 0.5 | 20 |

Table 5. 4 Upper power thresholds of DG for cases

| DG no. | Cases 1 and 2 | | Cases 3 and 4 | |
|---|---|---|---|---|
| | $P_{DGi}^{max}$ (kW) | $Q_{DGi}^{max}$ (kvar) | $P_{DGi}^{max}$ (kW) | $Q_{DGi}^{max}$ (kvar) |
| DG1 | 1750 | 1300 | 975 | 522.5 |
| DG2 | 950 | 440 | 850 | 517.5 |
| DG3 | 1400 | 800 | 825 | 510 |
| DG4 | – | – | 750 | 500 |
| DG5 | – | – | 700 | 490 |

Table 5. 5 Bottom and top thresholds of the DIMG working voltage frequency and magnitude, and the DG reference voltage magnitude for cases

| $f^{min}$ (pu) | $f^{max}$ (pu) | $\lvert V^{min} \rvert$ (pu) | $\lvert V^{max} \rvert$ (pu) | $\lvert V_{ref}^{min} \rvert$ (pu) | $\lvert V_{ref}^{max} \rvert$ (pu) |
|---|---|---|---|---|---|
| 0.99 | 1.0 | 0.95 | 1.05 | 1.0 | 1.02 |

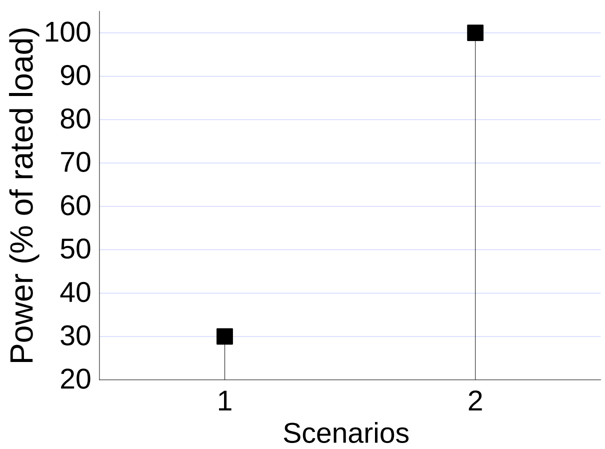


Fig. 5. 1 Load scenarios of the investigated load profile

### 5.3 Results and discussion

The suggested problem is conducted and experimented with using the MATLAB 2021a tool. The following is more detailed of the results and a discussion of the investigated cases. These findings are documented in [145].

#### 5.3.1 Case 1: Optimise the capacity of three DGs

Table 5. 6 Optimal droop parameters and reference frequency of DG (pu) for each technique

| Techniques | Parameters | DG1 | DG2 | DG3 |
|---|---|---|---|---|
| B-MOPSO [48] | $m_p$ | 0.001029 | 0.001467 | 0.001037 |
| | $n_q$ | 0.032205 | 0.044444 | 0.033333 |
| | $\|V_{ref}\|$ | 0.999758 | 1.020000 | 1.002497 |
| | $f_{ref}$ | 1.000900 | 0.999593 | 0.999641 |
| TV-MOPSO [146] | $m_p$ | 0.001111 | 0.001380 | 0.001125 |
| | $n_q$ | 0.031154 | 0.040534 | 0.030152 |
| | $\|V_{ref}\|$ | 1.020000 | 1.002900 | 1.020000 |
| | $f_{ref}$ | 1.000891 | 0.999543 | 0.999829 |
| NLTV-MOPSO [46] | $m_p$ | 0.001125 | 0.001351 | 0.001019 |
| | $n_q$ | 0.030373 | 0.042535 | 0.030000 |
| | $\|V_{ref}\|$ | 1.011400 | 1.014400 | 1.020000 |
| | $f_{ref}$ | 1.000880 | 0.999100 | 0.999250 |
| **DE (proposed)** | $m_p$ | –0.013700 | –0.032900 | –0.014800 |
| | $n_q$ | –0.058600 | –0.213100 | –0.063400 |
| | $\|V_{ref}\|$ | 1.012800 | 1.009100 | 1.020000 |
| | $f_{ref}$ | 1.000000 | 1.000000 | 1.000000 |

Table 5. 7 Optimal values of the working frequency in pu for various methods

| B-MOPSO [48] | TV-MOPSO [146] | NLTV-MOPSO [46] | **DE (proposed)** |
|---|---|---|---|
| 0.998304 | 0.998359 | 0.997930 | 0.990200 |

Table 5. 8 Droop-DG capacity and lost power of techniques

| | | B-MOPSO [48] | TV-MOPSO [146] | NLTV-MOPSO [46] | **DE (proposed)** |
|---|---|---|---|---|---|
| $P_{rated}$ (kW) | DG1 | 1600.00 | 1600.00 | 1600.00 | 1558.25 |
| | DG2 | 878.70 | 858.10 | 866.00 | 817.65 |
| | DG3 | 1289.00 | 1306.90 | 1298.40 | 1387.30 |
| | Sum | 3767.70 | 3765.00 | 3764.40 | 3763.20 |
| $Q_{rated}$ (kvar) | DG1 | 1200.00 | 1200.00 | 1200.00 | 1121.45 |
| | DG2 | 612.70 | 229.20 | 349.40 | 424.10 |
| | DG3 | 526.40 | 908.50 | 787.80 | 789.60 |
| | Sum | 2339.10 | 2337.70 | 2337.20 | 2335.15 |
| $P_{loss}$ (kW) | | 52.70 | 50.00 | 49.40 | **48.15** |
| $Q_{loss}$ (kvar) | | 39.20 | 37.70 | 37.20 | **36.45** |

In this work, the DE technique is introduced in order to identify the proper size of three droop-DGs within the suggested 33-bus DIMG grid at the nominal power load. The effectiveness of the suggested DE algorithm in Case 1 is compared with existing techniques, including B-MOPSO technique [48], Time-Varying MOPSO technique (TV-MOPSO) [146], and Non-Linear TV-MOPSO technique (NLTV-MOPSO) [46]. Table 5. 6 tabulates the parameters of three DGs, including the $f$ and $V$ droop gains, the reference voltage and frequency in each technique mentioned above. Table 5. 7

shows the frequency of the DIMG system related to each technique, with all values satisfying predetermined ranges.

Table 5. 8 shows the rated powers yielded by three DGs and the lost active and reactive power at the rated load for each technique. These optimally rated powers are computed through the tuned values of DG droop parameters (decision variables). As detailed in Table 5. 6, the proposed DE technique produces the best DG parameters, leading to the highest extent of the lost active and reactive power minimisation (Table 5. 8); in contrast, the B-MOPSO approach provides the worst (lowest) lost power mitigation due to its ineffective selection of parameters (Table 5. 8).

### 5.3.2 Case 2: Optimise the simultaneous capacity and positioning of three DGs

Table 5. 9 DG capacity and positioning and lost power of techniques

| **Techniques** | **DG No.** | **Optimal site** (bus) | **Capacity of DGs** | | **Power Losses** | |
|---|---|---|---|---|---|---|
| | | | $P_{rated}$ (kW) | $Q_{rated}$ (kvar) | $P_{loss}$ (kW) | $Q_{loss}$ (kvar) |
| CSI-IP [81] | DG1 | 13 | 680.00 | 421.40 | 30.40 | 23.40 |
| | DG2 | 24 | 1950.00 | 1208.00 | – | – |
| | DG3 | 29 | 1110.00 | 693.50 | – | – |
| CSI-PSO [81] | DG1 | 13 | 789.40 | 489.20 | 24.60 | 19.20 |
| | DG2 | 24 | 1551.90 | 961.80 | – | – |
| | DG3 | 29 | 1390.00 | 868.10 | – | – |
| **DE (proposed)** | DG1 | 23 | 1661.30 | 1109.60 | **23.90** | **18.85** |
| | DG2 | 13 | 863.35 | 407.35 | – | – |
| | DG3 | 30 | 1212.45 | 797.45 | – | – |

In this case, the DE technique is utilised to identify the simultaneous ideal positioning and size of three droop-DGs within the 33-bus DIMG test system that provide energy for the rated load. Table 5. 9 and Table 5. 10 detail the tuned values of the DG site and droop parameters (i.e., $m_{pi}$, $n_{qi}$, and $|V_{refi}|$) for control variables respectively, as mentioned in Section 5.1.1. When the droop parameters of three DGs are tuned, the optimal capacity of three DGs is achieved, which comprises the rated active and reactive power (Table 5. 9).

The suggested DE technique's efficacy for minimising lost power is tested by comparing it to the two current approaches, as listed in Table 5. 9, including Combined Sensitivity Index-Iterative Procedure technique (CSI-IP) [81], and CSI-PSO technique [81]. Data from Table 5. 9 indicate that the suggested DE approach is the most effective technique for mitigating power losses through the effective option of the droop gains, reference voltage, and placement of three DGs.

### 5.3.3 Comparison of lost active and reactive power minimisation between four cases

In this chapter, the effect of installing multiple droop-DG placements within the IMG system is considered to lower lost power in lines and gain nodal voltage. The load profile is set at the 30% and 100% levels of the rated load. Table 5. 10 tabulates the tuned parameters of the three and five droop-DGs using the suggested DE technique for four cases. Furthermore, all operating frequencies in each case are listed in Table 5. 11, where every frequency value conforms to the predetermined range.

Table 5. 12 shows a comparison of the objective functions (i.e., the lost active power and the reactive power loss) and the corresponding loss percentages for the deployment of three- and five-droop-DG placements in the investigated electric power system, accounting for site and/or size. Data from this table demonstrate that, compared to Case 1, which solely optimises the capacity of three droop-DGs and provides less desirable results because there is no optimal DG positioning (in contrast to Cases 2 and 4) and fewer DG sites (relative to Cases 3 and 4) than in other cases, Case 4 shows the most effective power loss minimisation. This case concerns

the optimisation of both the siting and sizing of five droop-DGs. Gupta et al. in Ref. [94] stated that an IMG's allowable range for lost active power is 0.5% to 1.5% of the rated load. With an outstanding 0.23% lost active power and 0.32% lost reactive power, Case 4 demonstrates superior performance among all cases.

Fig. 5. 2 illustrates the nodal voltage magnitudes of the above mentioned cases through the suggested DE algorithm at the rated load level. This figure makes it clear that Case 4 has the best voltage profile, since it gets the optimal number of droop-DG placements within the grid. On the contrary, Case 1 provides the magnitude values of the nodal voltage that are the least desired.

Table 5. 10 Droop parameters of DG (pu) for cases

| Cases | **Rated load** (%) | **Parameters** | **DG1** | **DG2** | **DG3** | **DG4** | **DG5** |
|---|---|---|---|---|---|---|---|
| 1 | 30 | $m_p$ | –0.0137 | –0.0329 | –0.0148 | – | – |
| | | $n_q$ | –0.0586 | –0.2131 | –0.0634 | – | – |
| | | $\|V_{ref}\|$ | 1.0128 | 1.0091 | 1.0200 | – | – |
| | 100 | $m_p$ | –0.0034 | –0.0068 | –0.0038 | – | – |
| | | $n_q$ | –0.0083 | –0.0294 | –0.0161 | – | – |
| | | $\|V_{ref}\|$ | 1.0196 | 1.0189 | 1.0189 | – | – |
| 2 | 30 | $m_p$ | –0.0116 | –0.0327 | –0.0209 | – | – |
| | | $n_q$ | –0.0474 | –0.2353 | –0.0649 | – | – |
| | | $\|V_{ref}\|$ | 1.0191 | 1.0041 | 1.0183 | – | – |
| | 100 | $m_p$ | –0.0032 | –0.0066 | –0.0044 | – | – |
| | | $n_q$ | –0.0098 | –0.0334 | –0.0160 | – | – |
| | | $\|V_{ref}\|$ | 1.0145 | 1.0186 | 1.0184 | – | – |
| 3 | 30 | $m_p$ | –0.0276 | –0.0372 | –0.0542 | –0.0394 | –0.0563 |
| | | $n_q$ | –0.2821 | –0.2918 | –0.5283 | –0.2180 | –0.1718 |
| | | $\|V_{ref}\|$ | 1.0009 | 1.0200 | 1.0059 | 1.0136 | 1.0168 |
| | 100 | $m_p$ | –0.0061 | –0.0073 | –0.0081 | –0.0081 | –0.0092 |
| | | $n_q$ | –0.0284 | –0.0276 | –0.0293 | –0.0279 | –0.0278 |
| | | $\|V_{ref}\|$ | 1.0186 | 1.0159 | 1.0098 | 1.0174 | 1.0141 |
| 4 | 30 | $m_p$ | –0.0331 | –0.0530 | –0.0417 | –0.0413 | –0.0375 |
| | | $n_q$ | –0.1586 | –0.1605 | –0.5149 | –0.2496 | –0.4471 |
| | | $\|V_{ref}\|$ | 1.0142 | 1.0191 | 1.0200 | 1.0025 | 1.0104 |
| | 100 | $m_p$ | –0.0066 | –0.0079 | –0.0073 | –0.0081 | –0.0091 |
| | | $n_q$ | –0.0269 | –0.0287 | –0.0285 | –0.0273 | –0.0291 |
| | | $\|V_{ref}\|$ | 1.0169 | 1.0182 | 1.0103 | 1.0166 | 1.0152 |

Table 5. 11 Values of the frequency of the system (pu) for the cases

| **Rated load** (%) | **Cases** | | | |
|---|---|---|---|---|
| | **1** | **2** | **3** | **4** |
| 30 | 0.9904 | 0.9901 | 0.9901 | 0.9901 |
| 100 | 0.9902 | 0.9900 | 0.9901 | 0.9900 |

Table 5. 12 Optimal number and placements of droop-DGs for four cases

| **Cases** | **DDG No.** | **Ideal site** (bus) | **Capacity of DDGs** | | **Power losses** | | **Percentage of losses** | |
|---|---|---|---|---|---|---|---|---|
| | | | $P_{rated}$ (kW) | $Q_{rated}$ (kvar) | $F_a$ (kW) | $F_b$ (kvar) | $P_{loss}$ (%) | $Q_{loss}$ (%) |
| 1 | DDG1 | | 1558.25 | 1121.45 | 52.20 | 39.55 | 1.08 | 1.32 |
| | DDG2 | | 817.65 | 424.10 | – | – | – | – |
| | DDG3 | | 1387.30 | 789.60 | – | – | – | – |
| 2 | DDG1 | 23 | 1661.30 | 1109.60 | 23.90 | 18.85 | 0.50 | 0.63 |
| | DDG2 | 13 | 863.35 | 407.35 | – | – | – | – |
| | DDG3 | 30 | 1212.45 | 797.45 | – | – | – | – |
| 3 | DDG1 | | 905.95 | 485.45 | 13.85 | 12.70 | 0.29 | 0.42 |
| | DDG2 | | 773.50 | 514.55 | – | – | – | – |
| | DDG3 | | 706.95 | 333.65 | – | – | – | – |
| | DDG4 | | 706.95 | 481.35 | – | – | – | – |
| | DDG5 | | 634.40 | 489.85 | – | – | – | – |
| **4** | DDG1 | 26 | 839.30 | 520.75 | **10.95** | **9.65** | **0.23** | **0.32** |
| | DDG2 | 31 | 736.35 | 510.00 | – | – | – | – |
| | DDG3 | 25 | 781.30 | 473.00 | – | – | – | – |
| | DDG4 | 2 | 712.75 | 430.90 | – | – | – | – |
| | DDG5 | 12 | 655.45 | 369.00 | – | – | – | – |

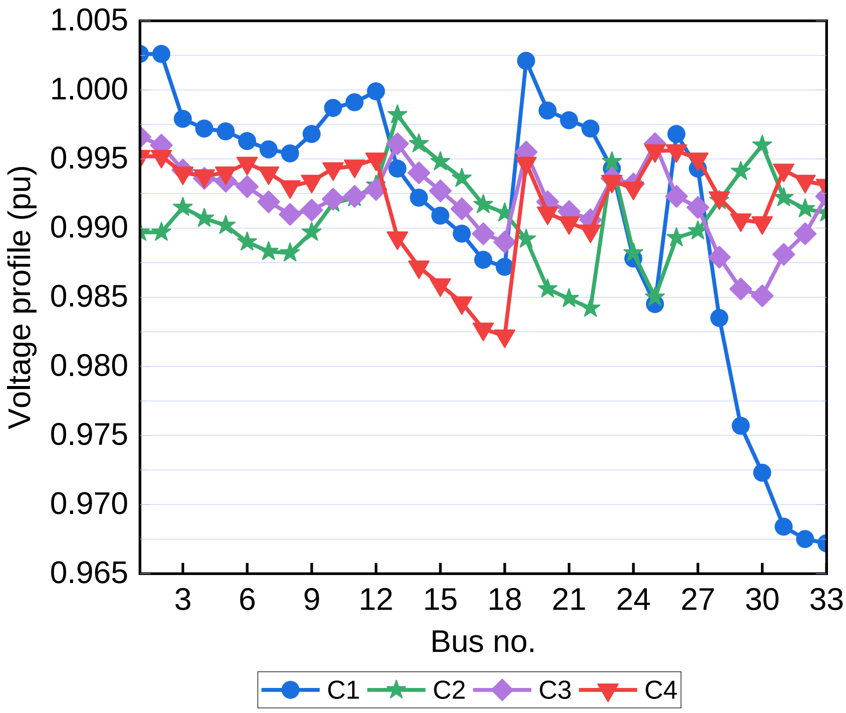


Fig. 5. 2 Voltage profile of four cases using the DE technique at the rated load

where: $Ci$ is the $i$-th Case with $i \in [1, 4]$.

## 5.4 Conclusion

In this chapter, the proper multiple droop-DG locations within the islanded microgrid are obtained to maximise lost power mitigation and increase the nodal voltage, taking into account load demands at minimum and maximum values (that is, 30% and 100%) of the rated capacity by the suggested DE approach. This technique is applied to tune the droop parameters (i.e., size) and the DG site, while the MBFS load flow approach is used to meet the operational requirements. The efficacy of the DE technique for the investigated cases is contrasted with some prior algorithms, including B-MOPSO, TV-MOPSO, NLTV-MOPSO, CSI-IP, and CSI-PSO. The simulation outcomes obtained point out that the suggested DE algorithm is efficient for the problem of deploying a number of droop-DGs to reduce lost power on the IMG grid (as presented in Tables 5. 8, 5. 9, and 5. 12). Furthermore, based on the findings in this chapter, it is demonstrated that when multiple droop-DG locations are optimised, power losses are considerably minimised, and bus voltage is improved, as shown in Case 4 of Table 5. 12 and Fig. 5. 2 respectively.

# CHAPTER 6

# CONCLUSIONS AND FUTURE STUDIES

Within the operation of DIMG networks, the uncertainty of the local load, coupled with the improper output power of the DG, leads to power mismatches. These mismatches give rise to inefficient energy use, where generation capacity exceeds demand, resulting in a reduction in power quality and impacting to voltage adjustment. Planning and mitigating power mismatches are necessary to guarantee the steady and dependable operation of the DIMGs. In order to resolve the issues mentioned above and achieve optimal DG planning in DIMGs, this thesis develops and suggests mathematical models, the optimal load flow method, and optimisation algorithms. The following is a summary of the key contributions presented in this thesis.

1. The author successfully applies the robust MBFS load flow approach to identify the ideal operational points in droop-based IMG, taking into account load variations over time for the proposed research.

2. The author develops Differential Evolution and Honey Badger-based metaheuristic algorithms to tune DG droop parameters and positioning in the islanded microgrid, which exhibit remarkable adaptability to changes in time-varying local load needs. Furthermore, the energy flow optimisation within the DIMG network is conducted through the MBFS approach. The results achieved after the simulation demonstrate that the HB technique is a reliable and robust technique for finding the proper capacity and site of droop-DGs

within the DIMG to reduce lost power and increase bus voltage. Moreover, the DIMG grid is assisted in lowering lost power and gaining bus voltage magnitude by simultaneous optimisation of the location and DG droop parameters.

3. The author implements multiple droop-DG placements with the aim of maximising lost active and reactive power minimisation while simultaneously increasing the nodal voltage in the IMG using the differential evolution technique, considering the variation of load demands at minimum and maximum values (i.e., 30% and 100%) of the nominal load level. The DE technique is applicable to optimise the droop parameters (i.e., sizing) and the DG positioning, while the MBFS approach is employed to satisfy operational constraints. The efficacy of the suggested DE technique for the investigated cases is compared with some established algorithms. The results obtained clearly demonstrate that the proposed DE algorithm is a robust and efficient technique for the problem of installing multiple droop-DG units.

The encouraging study findings described in this doctoral thesis suggest that other issues of operation, planning, and power system optimisation control can be tackled by using the suggested models, the optimal load flow method, and the optimisation algorithms. The following tasks are anticipated in the future.

1. The power grid is integrating renewable sources, like wind and solar-based DGs, more and more, driven by the more affordable generation costs and the reduced environmental impact. Therefore, optimising the allocation of DGs is crucial in an integrated DIMG consisting of these renewable generations.

2. To boost the penetration level of renewable generations within DNs, particularly in DIMG networks, future studies should consider the appropriate location and allocation of smart inverter devices, such as the PV plant, BESD, STATCOM, DSTATCOM, and PV-STATCOM for adaptive Volt-Var control (VVC).

3. Determining the optimal allocation of DRs operating in MGs is essential for transitioning between the on-grid and islanded modes of function. The purpose is to flexibly provide energy in order to meet the electrical demands throughout the MG operational process: a) MG can work within the autonomous mode when the national grid occurs intentional and unintentional issues, such as schedule maintenance and short circuits; b) In peak hours of RG and low local load, excess power of MG can inject into the national grid to minimise stress for the mentioned above smart inverter devices. On the contrary, the national grid provides energy to the local load when the microgrid is power-deficient due to reduced RGs throughout peak-off periods and high demand.

4. In practice, the operation of power girds with imbalanced three-phase networks is popular. As a result, performing the proper capacity and positioning of RGs under high penetration within IMG networks with imbalanced three-phase configurations is crucial for future research.

5. Mitigating distribution level losses and improving nodal voltages can be accomplished in a number of ways, including load balancing, installing

capacitors, reconfiguring a network, placing and numbering DG optimally, and raising voltage levels. This thesis mainly focusses on the suitable capacity and site of droop-DGs and the deployment of multiple droop-DG placements. The optimal simultaneous allocation (that is, size and site) of DRs and reconfigurable topology in IMGs significantly contribute to minimise lost power and improve nodal voltage. The future study should formulate an appropriate mathematical model to simultaneously optimise the allocation of DRs under a high penetration and reconfigurable topology, taking into account the presence of the mentioned smart inverter devices to obtain adaptive VVC.

6. In future studies, the deployment of a number of DR sites in IMGs is more than 30% of the total grid buses. This approach is significant with the aim of maximising lost power mitigation within the grid and gaining bus voltage.

# REFERENCES


[1] "Access to electricity – SDG7: Data and Projections – Analysis," IEA. Accessed: Aug. 29, 2023. [Online]. Available: https://www.iea.org/reports/sdg7-data-and-projections/access-to-electricity

[2] F. Katiraei, R. Iravani, N. Hatziargyriou, and A. Dimeas, "Microgrids management," *IEEE power and energy magazine*, vol. 6, no. 3, pp. 54–65, 2008.

[3] D. G. Photovoltaics and E. Storage, "IEEE standard for interconnection and interoperability of distributed energy resources with associated electric power systems interfaces," *IEEE Std*, pp. 1547–2018, 2018.

[4] A. Tomar, P. Gaur, R. Kandari, and N. Gupta, *Control of standalone microgrid*. Academic Press, 2021.

[5] D. H. Wolpert and W. G. Macready, "No free lunch theorems for optimization," *IEEE transactions on evolutionary computation*, vol. 1, no. 1, pp. 67–82, 1997.

[6] K. V. Price, "Differential evolution: a fast and simple numerical optimizer," in *Proceedings of North American fuzzy information processing*, IEEE, 1996, pp. 524–527.

[7] B. V. Kumar, D. Oliva, and P. N. Suganthan, *Differential Evolution: From Theory to Practice*. Springer, 2022.

[8] P. D. Huy, V. K. Ramachandaramurthy, J. Y. Yong, K. M. Tan, and J. B. Ekanayake, "Optimal placement, sizing and power factor of distributed generation: A comprehensive study spanning from the planning stage to the operation stage," *Energy*, vol. 195, p. 117011, 2020.

[9] A. M. Shaheen, R. A. El-Sehiemy, and S. M. Farrag, "A reactive power planning procedure considering iterative identification of VAR candidate buses," *Neural Computing and Applications*, vol. 31, pp. 653–674, 2019.

[10] P. A. Kumar, P. A. Jeyanthi, D. Devaraj, and G. M. Kurian, "Microgrid energy management using differential evolution algorithm," in *2018 International Conference on Advances in Computing, Communications and Informatics (ICACCI)*, IEEE, 2018, pp. 1280–1284.

[11] S. Zeynali, N. Rostami, and M. R. Feyzi, "Multi-objective optimal short-term planning of renewable distributed generations and capacitor banks in power system considering different uncertainties including plug-in electric vehicles," *International Journal of Electrical Power & Energy Systems*, vol. 119, p. 105885, 2020.

[12] V. Suresh and S. S. Kumar, "Optimal reactive power dispatch for minimization of real power loss using SBDE and DE-strategy algorithm," *Journal of Ambient Intelligence and Humanized Computing*, pp. 1–15, 2020.

[13] F. A. Hashim, E. H. Houssein, K. Hussain, M. S. Mabrouk, and W. Al-Atabany, "Honey Badger Algorithm: New metaheuristic algorithm for solving optimization problems," *Mathematics and Computers in Simulation*, vol. 192, pp. 84–110, 2022.

[14] S. N. Qasem, "A novel honey badger algorithm with multilayer perceptron for predicting COVID-19 time series data," *The Journal of Supercomputing*, pp. 1–27, 2023.

[15] I. H. Abdulqadder, D. Zou, and I. T. Aziz, "The DAG blockchain: A secure edge assisted honeypot for attack detection and multi-controller based load balancing in SDN 5G," *Future Generation Computer Systems*, vol. 141, pp. 339–354, 2023.

[16] P. Narmatha, S. Gupta, T. V. Lakshmi, and D. Manikavelan, "Skin cancer detection from dermoscopic images using Deep Siamese domain adaptation convolutional Neural Network optimized with Honey Badger Algorithm," *Biomedical Signal Processing and Control*, vol. 86, p. 105264, 2023.

[17] M. Thirunavukkarasu, H. Lala, and Y. Sawle, "Techno-economic-environmental analysis of off-grid hybrid energy systems using honey badger optimizer," *Renewable Energy*, vol. 218, p. 119247, 2023.

[18] E. Akbari, N. Shafaghatian, F. Zishan, O. D. Montoya, and D. A. Giral-Ramírez, "Optimized two-level control of islanded microgrids to reduce fluctuations," *IEEE Access*, vol. 10, pp. 95824–95838, 2022.

[19] A. Fathy, H. Rezk, S. Ferahtia, R. M. Ghoniem, and R. Alkanhel, "An efficient honey badger algorithm for scheduling the microgrid energy management," *Energy Reports*, vol. 9, pp. 2058–2074, 2023.

[20] N. A. Kamarzaman, S. I. Sulaiman, A. I. M. Yassin, I. R. Ibrahim, and H. Zainuddin, "A honey badger algorithm for optimal sizing of an AC coupled hybrid stand-alone photovoltaic system," *Energy Reports*, vol. 8, pp. 511–520, 2022.

[21] G. K. Jaiswal, U. Nangia, and N. K. Jain, "Optimal Reactive Power Dispatch Using Honey Badger algorithm (HBA)," in *2022 IEEE 10th Power India International Conference (PIICON)*, IEEE, 2022, pp. 1–6.

[22] R. K. Khadanga, S. R. Nayak, S. Panda, D. Das, B. R. Prusty, and P. R. Sahu, "A Novel Optimal Robust Design Method for Frequency Regulation of Three-Area Hybrid Power System Utilizing Honey Badger Algorithm," *International Transactions on Electrical Energy Systems*, vol. 2022, 2022.

[23] F. Hameed, M. Al Hosani, and H. H. Zeineldin, "A modified backward/forward sweep load flow method for islanded radial microgrids," *IEEE Transactions on Smart Grid*, vol. 10, no. 1, pp. 910–918, 2017.

[24] M. Basu, "Dynamic optimal power flow for isolated microgrid incorporating renewable energy sources," *Energy*, vol. 264, p. 126065, 2023.

[25] K. Hesaroor and D. Das, “Improved Modified Newton Raphson Load Flow Method for Islanded Microgrids,” in *2020 IEEE 17th India Council International Conference (INDICON)*, IEEE, 2020, pp. 1–6.

[26] A. Uniyal and S. Sarangi, “Optimal allocation of ELC in microgrid using droop controlled load flow,” *IET Generation, Transmission & Distribution*, vol. 13, no. 20, pp. 4566–4578, 2019.

[27] A. Uniyal, S. Sarangi, and M. S. Rawat, “Optimal Dump Load Allocations in High RBDG Penetrated Microgrid for Voltage and Frequency Regulation,” *Arabian Journal for Science and Engineering*, vol. 46, no. 2, pp. 1511–1528, 2021.

[28] M. Z. Kreishan and A. F. Zobaa, “Allocation of Dump Load in Islanded Microgrid Using the Mixed-Integer Distributed Ant Colony Optimization,” *IEEE Systems Journal*, 2021.

[29] D. Liu, C. Zhang, Y. Xu, Z. Dong, and Y. Chi, “Sensitivity Region Based Optimization for Maximiz-ing Renewable Generation Hosting Capacity of An Islanded Microgrid,” *IEEE Transactions on Smart Grid*, 2022.

[30] S. Ashfaq, D. Zhang, C. Zhang, and Z. Y. Dong, “Load flow investigations for regionalized islanded microgrid considering frequency regulation with high renewable penetration,” *Electric Power Systems Research*, vol. 214, p. 108904, 2023.

[31] T. L. Vandoorn, B. Meersman, J. D. De Kooning, and L. Vandevelde, “Analogy between conventional grid control and islanded microgrid control based on a global DC-link voltage droop,” *IEEE transactions on power delivery*, vol. 27, no. 3, pp. 1405–1414, 2012.

[32] F. Blaabjerg, *Control of Power Electronic Converters and Systems: Volume 2*, vol. 2. Academic Press, 2018.

[33] M. V. Kirthiga, S. A. Daniel, and S. Gurunathan, “A methodology for transforming an existing distribution network into a sustainable autonomous micro-grid,” *IEEE Transactions on Sustainable Energy*, vol. 4, no. 1, pp. 31–41, 2012.

[34] E. Fouladi, H. R. Baghaee, M. Bagheri, M. Lu, and G. B. Gharehpetian, “BESS Sizing in an Isolated Microgrid Including PHEVs and RERs,” in *2020 IEEE International Conference on Environment and Electrical Engineering and 2020 IEEE Industrial and Commercial Power Systems Europe (EEEIC/I&CPS Europe)*, IEEE, 2020, pp. 1–5.

[35] V. Guliashki and G. Marinova, “Optimization of Energy Storage Capacity in an Islanded Microgrid,” in *Proc. of ICEST’2017 (Editor Prof. Dr. Milovanovic, B.), 2017, Niš, Serbia*, 2017, pp. 329–332.

[36] S. Y. Lee, Y. G. Jin, and Y. T. Yoon, “Determining the optimal reserve capacity in a microgrid with islanded operation,” *IEEE Transactions on Power Systems*, vol. 31, no. 2, pp. 1369–1376, 2015.

[37] T. Kerdphol, K. Fuji, Y. Mitani, M. Watanabe, and Y. Qudaih, "Optimization of a battery energy storage system using particle swarm optimization for stand-alone microgrids," *International Journal of Electrical Power & Energy Systems*, vol. 81, pp. 32–39, 2016.

[38] K. A. Kavadias, D. Apostolou, and J. K. Kaldellis, "Modelling and optimisation of a hydrogen-based energy storage system in an autonomous electrical network," *Applied energy*, vol. 227, pp. 574–586, 2018.

[39] S. M. Sadek, W. A. Omran, M. M. Hassan, and H. E. Talaat, "Adaptive robust energy management for isolated microgrids considering reactive power capabilities of distributed energy resources and reactive power costs," *Electric Power Systems Research*, vol. 199, p. 107375, 2021.

[40] R. Xie, W. Wei, M. Shahidehpour, Q. Wu, and S. Mei, "Sizing Renewable Generation and Energy Storage in Stand-Alone Microgrids Considering Distributionally Robust Shortfall Risk," *IEEE Transactions on Power Systems*, 2022.

[41] C.-T. Tsai, T. M. Beza, E. M. Molla, and C.-C. Kuo, "Analysis and sizing of mini-grid hybrid renewable energy system for islands," *IEEE Access*, vol. 8, pp. 70013–70029, 2020.

[42] J. Xiao, L. Bai, F. Li, H. Liang, and C. Wang, "Sizing of energy storage and diesel generators in an isolated microgrid using discrete Fourier transform (DFT)," *IEEE Transactions on Sustainable Energy*, vol. 5, no. 3, pp. 907–916, 2014.

[43] B. Mukhopadhyay and D. Das, "Optimal multi-objective expansion planning of a droop-regulated islanded microgrid," *Energy*, vol. 218, p. 119415, 2021.

[44] N. B. Roy and D. Das, "Optimal allocation of active and reactive power of dispatchable distributed generators in a droop controlled islanded microgrid considering renewable generation and load demand uncertainties," *Sustainable Energy, Grids and Networks*, vol. 27, p. 100482, 2021.

[45] L. Subramanian, V. Debusschere, and H. B. Gooi, "Design and control of storage systems for voltage source controlled autonomous microgrids," in *2019 IEEE Power & Energy Society General Meeting (PESGM)*, IEEE, 2019, pp. 1–5.

[46] J. Jithendranath and D. Das, "Multi-objective optimal power flow in islanded microgrids with solar PV generation by NLTV-MOPSO," *IETE Journal of Research*, vol. 69, no. 4, pp. 2130–2143, 2023.

[47] A. Maulik and D. Das, "Optimal operation of a droop-controlled DCMG with generation and load uncertainties," *IET Generation, Transmission & Distribution*, vol. 12, no. 12, pp. 2905–2917, 2018.

[48] A. Maulik and D. Das, "Optimal operation of droop-controlled islanded microgrids," *IEEE Transactions on Sustainable Energy*, vol. 9, no. 3, pp. 1337–1348, 2017.

[49] M. R. Aghamohammadi and H. Abdolahinia, “A new approach for optimal sizing of battery energy storage system for primary frequency control of islanded microgrid,” *International Journal of Electrical Power & Energy Systems*, vol. 54, pp. 325–333, 2014.

[50] K. S. El-Bidairi, H. D. Nguyen, T. S. Mahmoud, S. D. G. Jayasinghe, and J. M. Guerrero, “Optimal sizing of Battery Energy Storage Systems for dynamic frequency control in an islanded microgrid: A case study of Flinders Island, Australia,” *Energy*, vol. 195, p. 117059, 2020.

[51] J. M. Rey, I. Jiménez-Vargas, P. P. Vergara, G. Osma-Pinto, and J. Solano, “Sizing of an autonomous microgrid considering droop control,” *International Journal of Electrical Power & Energy Systems*, vol. 136, p. 107634, 2022.

[52] G. Diaz, C. Gonzalez-Moran, J. Gomez-Aleixandre, and A. Diez, “Scheduling of droop coefficients for frequency and voltage regulation in isolated microgrids,” *IEEE Transactions on Power Systems*, vol. 25, no. 1, pp. 489–496, 2009.

[53] M. A. Shoeb, F. Shahnia, and G. Shafiullah, “A multilayer optimization scheme to retain the voltage and frequency in standalone microgrids,” in *2017 IEEE Innovative Smart Grid Technologies - Asia (ISGT-Asia)*, Auckland: IEEE, Dec. 2017, pp. 1–6.

[54] M. M. A. Abdelaziz, H. E. Farag, and E. F. El-Saadany, “Optimum droop parameter settings of islanded microgrids with renewable energy resources,” *IEEE Transactions on Sustainable Energy*, vol. 5, no. 2, pp. 434–445, 2014.

[55] A. Yavuz, N. Celik, C.-H. Chen, and J. Xu, “A Sequential Sampling-based Particle Swarm Optimization to Control Droop Coefficients of Distributed Generation Units in Microgrid Clusters,” *Electric power systems research*, vol. 216, p. 109074, 2023.

[56] D. Manna, S. K. Goswami, and P. K. Chattopadhyay, “Optimisation of droop coefficients of multiple distributed generators in a micro-grid,” *IET Generation, Transmission & Distribution*, vol. 12, no. 18, pp. 4108–4116, 2018.

[57] H. R. Pota, “Droop control for islanded microgrids,” in *2013 IEEE Power & Energy Society General Meeting*, IEEE, 2013, pp. 1–4.

[58] M. Minetti, A. Rosini, G. B. Denegri, A. Bonfiglio, and R. Procopio, “An advanced droop control strategy for reactive power: assessment in islanded microgrids,” *IEEE Transactions on Power Systems*, 2021.

[59] C. L. Masters, “Voltage rise: the big issue when connecting embedded generation to long 11 kV overhead lines,” *Power engineering journal*, vol. 16, no. 1, pp. 5–12, 2002.

[60] A. Canova, L. Giaccone, F. Spertino, and M. Tartaglia, “Electrical impact of photovoltaic plant in distributed network,” *IEEE Transactions on industry applications*, vol. 45, no. 1, pp. 341–347, 2009.

[61] M. N. Kabir, Y. Mishra, G. Ledwich, Z. Y. Dong, and K. P. Wong, "Coordinated Control of Grid-Connected Photovoltaic Reactive Power and Battery Energy Storage Systems to Improve the Voltage Profile of a Residential Distribution Feeder," *IEEE Trans. Ind. Inf.*, vol. 10, no. 2, pp. 967–977, May 2014.

[62] M. Uddin, M. F. Romlie, M. F. Abdullah, C. Tan, G. M. Shafiullah, and A. H. A. Bakar, "A novel peak shaving algorithm for islanded microgrid using battery energy storage system," *Energy*, vol. 196, p. 117084, 2020.

[63] A. Arcos-Vargas, D. Lugo, and F. Núñez, "Residential peak electricity management. A storage and control systems application taking advantages of smart meters," *International Journal of Electrical Power & Energy Systems*, vol. 102, pp. 110–121, 2018.

[64] M. M. Rana, M. F. Romlie, M. F. Abdullah, M. Uddin, and M. R. Sarkar, "A novel peak load shaving algorithm for isolated microgrid using hybrid PV-BESS system," *Energy*, vol. 234, p. 121157, 2021.

[65] U. T. Salman, F. S. Al-Ismail, and M. Khalid, "Optimal sizing of battery energy storage for grid-connected and isolated wind-penetrated microgrid," *IEEE Access*, vol. 8, pp. 91129–91138, 2020.

[66] M. V. Kirthiga and S. A. Daniel, "Optimal sizing of hybrid generators for autonomous operation of a micro-grid," in *2010 IEEE 26-th Convention of Electrical and Electronics Engineers in Israel*, IEEE, 2010, pp. 000864–000868.

[67] S. X. Chen, H. B. Gooi, and M. Wang, "Sizing of energy storage for microgrids," *IEEE transactions on smart grid*, vol. 3, no. 1, pp. 142–151, 2011.

[68] H. Khorramdel, J. Aghaei, B. Khorramdel, and P. Siano, "Optimal battery sizing in microgrids using probabilistic unit commitment," *IEEE Transactions on Industrial Informatics*, vol. 12, no. 2, pp. 834–843, 2015.

[69] M. Vahedipour-Dahraei, H. R. Najafi, A. Anvari-Moghaddam, and J. M. Guerrero, "Security-constrained unit commitment in AC microgrids considering stochastic price-based demand response and renewable generation," *International Transactions on Electrical Energy Systems*, vol. 28, no. 9, p. e2596, 2018.

[70] M. Sufyan, N. Abd Rahim, C. Tan, M. A. Muhammad, and S. R. Sheikh Raihan, "Optimal sizing and energy scheduling of isolated microgrid considering the battery lifetime degradation," *PloS one*, vol. 14, no. 2, p. e0211642, 2019.

[71] Y. Qiu, Q. Li, S. Zhao, and W. Chen, "Planning optimization for islanded microgrid with electric-hydrogen hybrid energy storage system based on electricity cost and power supply reliability," in *Renewable Energy Microgeneration Systems*, Elsevier, 2021, pp. 49–67.

[72] H. Alharbi and K. Bhattacharya, "Stochastic optimal planning of battery energy storage systems for isolated microgrids," *IEEE Transactions on Sustainable Energy*, vol. 9, no. 1, pp. 211–227, 2017.

[73] M. Zolfaghari, N. Ghaffarzadeh, and A. J. Ardakani, “Optimal sizing of battery energy storage systems in off-grid micro grids using convex optimization,” *Journal of Energy Storage*, vol. 23, pp. 44–56, 2019.

[74] K. Hesaroor and D. Das, “Optimal sizing of energy storage system in islanded microgrid using incremental cost approach,” *Journal of Energy storage*, vol. 24, p. 100768, 2019.

[75] R. Khezri, A. Mahmoudi, and M. H. Haque, “A demand side management approach for optimal sizing of standalone renewable-battery systems,” *IEEE Transactions on Sustainable Energy*, vol. 12, no. 4, pp. 2184–2194, 2021.

[76] M. Combe, A. Mahmoudi, M. H. Haque, and R. Khezri, “Optimal sizing of an AC-coupled hybrid power system considering incentive-based demand response,” *IET Generation, Transmission & Distribution*, vol. 13, no. 15, pp. 3354–3361, 2019.

[77] T. Khalili, A. Jafari, M. Abapour, and B. Mohammadi-Ivatloo, “Optimal battery technology selection and incentive-based demand response program utilization for reliability improvement of an insular microgrid,” *Energy*, vol. 169, pp. 92–104, 2019.

[78] M. K. Kiptoo, M. E. Lotfy, O. B. Adewuyi, A. Conteh, A. M. Howlader, and T. Senjyu, “Integrated approach for optimal techno-economic planning for high renewable energy-based isolated microgrid considering cost of energy storage and demand response strategies,” *Energy Conversion and Management*, vol. 215, p. 112917, 2020.

[79] A. Arabali, M. Ghofrani, M. Etezadi-Amoli, and M. S. Fadali, “Stochastic performance assessment and sizing for a hybrid power system of solar/wind/energy storage,” *IEEE Transactions on Sustainable Energy*, vol. 5, no. 2, pp. 363–371, 2013.

[80] M. P. Anand, W. Ongsakul, J. G. Singh, and K. M. Sudhesh, “Optimal allocation and sizing of distributed generators in autonomous microgrids based on LSF and PSO,” in *2015 International Conference on Energy Economics and Environment (ICEEE)*, IEEE, 2015, pp. 1–6.

[81] R. Hari Kumar, N. Mayadevi, V. P. Mini, and S. Ushakumari, “Transforming distribution system into a sustainable isolatedmicrogrid considering contingency,” *Bulletin of the Polish Academy of Sciences. Technical Sciences*, vol. 67, no. 5, 2019.

[82] A. A. Anderson and S. Suryanarayanan, “Review of energy management and planning of islanded microgrids,” *CSEE Journal of Power and Energy Systems*, vol. 6, no. 2, pp. 329–343, 2019.

[83] S. Kayalvizhi and D. V. Kumar, “Optimal operation of autonomous microgrid for minimization of energy loss, cost and voltage deviation,” in *2015 IEEE Workshop on Computational Intelligence: Theories, Applications and Future Directions (WCI)*, IEEE, 2015, pp. 1–6.

[84] L. Guo, N. Wang, H. Lu, X. Li, and C. Wang, "Multi-objective optimal planning of the stand-alone microgrid system based on different benefit subjects," *Energy*, vol. 116, pp. 353–363, Dec. 2016.

[85] X. Feng, J. Gu, and X. Guan, "Optimal allocation of hybrid energy storage for microgrids based on multi-attribute utility theory," *Journal of Modern Power Systems and Clean Energy*, vol. 6, no. 1, pp. 107–117, 2018.

[86] A. Hussain, S. D. A. Shah, and S. M. Arif, "Heuristic optimisation-based sizing and siting of DGs for enhancing resiliency of autonomous microgrid networks," *IET Smart Grid*, vol. 2, no. 2, pp. 269–282, 2019.

[87] A. Hussain, S. M. Arif, M. Aslam, and S. D. A. Shah, "Optimal siting and sizing of tri-generation equipment for developing an autonomous community microgrid considering uncertainties," *Sustainable Cities and Society*, vol. 32, pp. 318–330, 2017.

[88] A. Ali, K. Mahmoud, and M. Lehtonen, "Optimization of photovoltaic and wind generation systems for autonomous microgrids with PEV-parking lots," *IEEE Systems Journal*, vol. 16, no. 2, pp. 3260–3271, 2021.

[89] A. Ali, K. Mahmoud, and M. Lehtonen, "Optimal planning of inverter-based renewable energy sources towards autonomous microgrids accommodating electric vehicle charging stations," *IET Generation, Transmission & Distribution*, vol. 16, no. 2, pp. 219–232, 2022.

[90] C. D. Rodríguez-Gallegos, D. Yang, O. Gandhi, M. Bieri, T. Reindl, and S. K. Panda, "A multi-objective and robust optimization approach for sizing and placement of PV and batteries in off-grid systems fully operated by diesel generators: An Indonesian case study," *Energy*, vol. 160, pp. 410–429, 2018.

[91] S. Ashfaq, D. Zhang, C. Zhang, and Z. Y. Dong, "Regionalisation of islanded microgrid considering planning and operation stages," *IET Renewable Power Generation*, vol. 14, no. 1, pp. 145–153, Jan. 2020.

[92] A. Uniyal and S. Sarangi, "Optimal DG allocation in a microgrid using droop-controlled load flow," in *Intelligent Computing Techniques for Smart Energy Systems*, Springer, 2020, pp. 745–752.

[93] M. F. Shaaban, A. Saber, M. E. Ammar, and H. H. Zeineldin, "A multi-objective planning approach for optimal DG allocation for droop based microgrids," *Electric Power Systems Research*, vol. 200, p. 107474, 2021.

[94] Y. Gupta, S. Doolla, K. Chatterjee, and B. C. Pal, "Optimal DG allocation and Volt–Var dispatch for a droop-based microgrid," *IEEE Transactions on Smart Grid*, vol. 12, no. 1, pp. 169–181, 2020.

[95] Y. Gupta, R. Nellikkath, K. Chatterjee, and S. Doolla, "Volt–Var Optimization and Reconfiguration: Reducing Power Demand and Losses in a Droop-Based

Microgrid," *IEEE Transactions on Industry Applications*, vol. 57, no. 3, pp. 2769–2781, 2021.

[96] H. Moazami Goodarzi and M. H. Kazemi, "An optimal autonomous microgrid cluster based on distributed generation droop parameter optimization and renewable energy sources using an improved grey wolf optimizer," *Engineering Optimization*, vol. 50, no. 5, pp. 819–839, 2018.

[97] V. B. Foroutan, M. H. Moradi, and M. Abedini, "Optimal operation of autonomous microgrid including wind turbines," *Renewable Energy*, vol. 99, pp. 315–324, 2016.

[98] A. H. Yazdavar, M. F. Shaaban, E. F. El-Saadany, M. M. Salama, and H. H. Zeineldin, "Optimal planning of distributed generators and shunt capacitors in isolated microgrids with nonlinear loads," *IEEE Transactions on Sustainable Energy*, vol. 11, no. 4, pp. 2732–2744, 2020.

[99] A. S. Awad, T. H. El-Fouly, and M. M. Salama, "Optimal ESS allocation and load shedding for improving distribution system reliability," *IEEE Transactions on Smart Grid*, vol. 5, no. 5, pp. 2339–2349, 2014.

[100] M. V. Castro, C. Moreira, and L. M. Carvalho, "Hierarchical optimisation strategy for energy scheduling and volt/var control in autonomous clusters of microgrids," *IET Renewable Power Generation*, vol. 14, no. 1, pp. 27–38, 2020.

[101] M. Khalid, U. Akram, and S. Shafiq, "Optimal planning of multiple distributed generating units and storage in active distribution networks," *IEEE Access*, vol. 6, pp. 55234–55244, 2018.

[102] M. Ramírez, R. Castellanos, G. Calderón, and O. Malik, "Placement and sizing of battery energy storage for primary frequency control in an isolated section of the Mexican power system," *Electric Power Systems Research*, vol. 160, pp. 142–150, 2018.

[103] K. Hesaroor and D. Das, "Optimal siting and sizing of batteries in radial autonomous microgrids considering congestion," in *IECON 2019-45th Annual Conference of the IEEE Industrial Electronics Society*, IEEE, 2019, pp. 5820–5825.

[104] I. Miranda, N. Silva, and H. Leite, "A holistic approach to the integration of battery energy storage systems in island electric grids with high wind penetration," *IEEE Transactions on Sustainable Energy*, vol. 7, no. 2, pp. 775–785, 2015.

[105] J. Qiu, J. Zhao, Y. Zheng, Z. Dong, and Z. Y. Dong, "Optimal allocation of BESS and MT in a microgrid," *IET Generation, Transmission & Distribution*, vol. 12, no. 9, pp. 1988–1997, May 2018.

[106] F. Samadi Gazijahani and J. Salehi, "Stochastic multi-objective framework for optimal dynamic planning of interconnected microgrids," *IET Renewable Power Generation*, vol. 11, no. 14, pp. 1749–1759, Dec. 2017.

[107] Q. Sun, B. Huang, D. Li, D. Ma, and Y. Zhang, "Optimal placement of energy storage devices in microgrids via structure preserving energy function," *IEEE Transactions on Industrial Informatics*, vol. 12, no. 3, pp. 1166–1179, 2016.

[108] M. H. Parvaneh, M. H. Moradi, and S. M. Azimi, "The advantages of capacitor bank placement and demand response program execution on the optimal operation of isolated microgrids," *Electric Power Systems Research*, vol. 220, p. 109345, 2023.

[109] H. E. Farag and E. F. El-Saadany, "Optimum shunt capacitor placement in multimicrogrid systems with consideration of islanded mode of operation," *IEEE Transactions on Sustainable Energy*, vol. 6, no. 4, pp. 1435–1446, 2015.

[110] R. Gholami, M. Shahabi, and M.-R. Haghifam, "An efficient optimal capacitor allocation in DG embedded distribution networks with islanding operation capability of micro-grid using a new genetic based algorithm," *International Journal of Electrical Power & Energy Systems*, vol. 71, pp. 335–343, 2015.

[111] A. Naderipour *et al.*, "Spotted hyena optimizer algorithm for capacitor allocation in radial distribution system with distributed generation and microgrid operation considering different load types," *Scientific reports*, vol. 11, no. 1, pp. 1–15, 2021.

[112] A. R. Salehinia, M. R. Haghifam, and M. Shahabi, "Volt/Var control in a microgrid with consideration of uncertainty of generation in both grid-connected and islanded modes of operation," in *CIRED 2012 Workshop: Integration of Renewables into the Distribution Grid*, Lisbon, Portugal: IET, 2012, pp. 191–191.

[113] H. M. El Zoghby and H. S. Ramadan, "Isolated microgrid stability reinforcement using optimally controlled STATCOM," *Sustainable Energy Technologies and Assessments*, vol. 50, p. 101883, 2022.

[114] Z. Wang, B. Chen, J. Wang, J. Kim, and M. M. Begovic, "Robust optimization based optimal DG placement in microgrids," *IEEE Transactions on Smart Grid*, vol. 5, no. 5, pp. 2173–2182, 2014.

[115] S. Ray, A. Bhattacharya, and S. Bhattacharjee, "Optimal allocation of distributed generation and remote control switches for reliability enhancement of a radial distribution system using oppositional differential search algorithm," *J. eng.*, vol. 2015, no. 8, pp. 261–275.

[116] C. H. Antunes, D. F. Pires, C. Barrico, A. Gomes, and A. G. Martins, "A multi-objective evolutionary algorithm for reactive power compensation in distribution networks," *Applied Energy*, vol. 86, no. 7–8, pp. 977–984, 2009.

[117] K. Sivakumar, R. Jayashree, and K. Danasagaran, "Efficiency-driven planning for sizing of distributed generators and optimal construction of a cluster of microgrids," *Engineering Science and Technology, an International Journal*, 2021.

[118] D. Singh, D. Singh, and K. Verma, "Multiobjective optimization for DG planning with load models," *IEEE transactions on power systems*, vol. 24, no. 1, pp. 427–436, 2009.

[119] H. Hedayati, S. A. Nabaviniaki, and A. Akbarimajd, "A method for placement of DG units in distribution networks," *IEEE transactions on power delivery*, vol. 23, no. 3, pp. 1620–1628, 2008.

[120] D. Q. Hung and N. Mithulananthan, "Multiple distributed generator placement in primary distribution networks for loss reduction," *IEEE Transactions on industrial electronics*, vol. 60, no. 4, pp. 1700–1708, 2011.

[121] D. B. Prakash and C. Lakshminarayana, "Multiple DG placements in distribution system for power loss reduction using PSO algorithm," *Procedia technology*, vol. 25, pp. 785–792, 2016.

[122] D. Rath, S. Halder Nee Dey, and S. K. Goswami, "Optimal Inverter-Based DG Placement considering Energy Loss, Reliability, Voltage Sag, DG, and Substation Power Cost Issues," *Electric Power Components and Systems*, vol. 51, no. 5, pp. 409–420, Mar. 2023.

[123] S. Das, D. Das, and A. Patra, "Operation of distribution network with optimal placement and sizing of dispatchable DGs and shunt capacitors," *Renewable and Sustainable Energy Reviews*, vol. 113, p. 109219, 2019.

[124] Z. M. Anjum, D. M. Said, M. Y. Hassan, Z. H. Leghari, and G. Sahar, "Parallel operated hybrid Arithmetic-Salp swarm optimizer for optimal allocation of multiple distributed generation units in distribution networks," *Plos one*, vol. 17, no. 4, p. e0264958, 2022.

[125] H. U. R. Habib *et al.*, "Optimal Placement and Sizing Problem for Power Loss Minimization and Voltage Profile Improvement of Distribution Networks under Seasonal Loads Using Harris Hawks Optimizer," *International Transactions on Electrical Energy Systems*, vol. 2022, 2022.

[126] T. R. Ayodele, A. S. O. Ogunjuyigbe, and O. O. Akinola, "Optimal location, sizing, and appropriate technology selection of distributed generators for minimizing power loss using genetic algorithm," *Journal of Renewable Energy*, vol. 2015, 2015.

[127] A. Waqar *et al.*, "Analysis of optimal deployment of several DGs in distribution networks using plant propagation algorithm," *IEEE Access*, vol. 8, pp. 175546–175562, 2020.

[128] A. Selim, S. Kamel, and F. Jurado, "Efficient optimization technique for multiple DG allocation in distribution networks," *Applied Soft Computing*, vol. 86, p. 105938, 2020.

[129] T. X. Nguyen and R. Lis, "Optimal size and location of dispatchable distributed generators in an autonomous microgrid using Honey Badger algorithm," *Archives of Electrical Engineering*, pp. 871–893, 2023.

[130] K. Price, R. M. Storn, and J. A. Lampinen, *Differential evolution: a practical approach to global optimization*. Springer Science & Business Media, 2006.

[131] E. S. Song and H. Li, “A hybrid differential evolution for multi-objective optimisation problems,” *Connection Science*, pp. 1–30, 2021.

[132] S. Rahnamayan, H. R. Tizhoosh, and M. M. Salama, “Opposition-based differential evolution,” *IEEE Transactions on Evolutionary computation*, vol. 12, no. 1, pp. 64–79, 2008.

[133] S. Das, A. Konar, and U. K. Chakraborty, “Improved differential evolution algorithms for handling noisy optimization problems,” in *2005 IEEE Congress on Evolutionary Computation*, Sep. 2005, pp. 1691-1698 Vol. 2.

[134] P. Kundur, *Power System Stability and Control*, 1st edition. New York: McGraw-Hill Education, 1994.

[135] J. P. Lopes, C. L. Moreira, and A. G. Madureira, “Defining control strategies for microgrids islanded operation,” *IEEE Transactions on power systems*, vol. 21, no. 2, pp. 916–924, 2006.

[136] W. Yao, M. Chen, J. Matas, J. M. Guerrero, and Z.-M. Qian, “Design and analysis of the droop control method for parallel inverters considering the impact of the complex impedance on the power sharing,” *IEEE Transactions on Industrial Electronics*, vol. 58, no. 2, pp. 576–588, 2010.

[137] J. M. Guerrero, J. Matas, L. G. de Vicuna, M. Castilla, and J. Miret, “Decentralized control for parallel operation of distributed generation inverters using resistive output impedance,” *IEEE Transactions on industrial electronics*, vol. 54, no. 2, pp. 994–1004, 2007.

[138] H. Bevrani and S. Shokoohi, “An intelligent droop control for simultaneous voltage and frequency regulation in islanded microgrids,” *IEEE transactions on smart grid*, vol. 4, no. 3, pp. 1505–1513, 2013.

[139] J. C. Vasquez, J. M. Guerrero, M. Savaghebi, J. Eloy-Garcia, and R. Teodorescu, “Modeling, analysis, and design of stationary-reference-frame droop-controlled parallel three-phase voltage source inverters,” *IEEE Transactions on industrial electronics*, vol. 60, no. 4, pp. 1271–1280, 2012.

[140] E. Planas, A. Gil-de-Muro, J. Andreu, I. Kortabarria, and I. M. de Alegría, “General aspects, hierarchical controls and droop methods in microgrids: A review,” *Renewable and Sustainable Energy Reviews*, vol. 17, pp. 147–159, 2013.

[141] J.-H. Teng, “A direct approach for distribution system load flow solutions,” *IEEE Transactions on power delivery*, vol. 18, no. 3, pp. 882–887, 2003.

[142] A. C. Lisboa, L. S. M. Guedes, D. A. G. Vieira, and R. R. Saldanha, “A fast power flow method for radial networks with linear storage and no matrix inversions,” *International Journal of Electrical Power & Energy Systems*, vol. 63, pp. 901–907, 2014.

[143] M. Chakravorty and D. Das, “Voltage stability analysis of radial distribution networks,” *International Journal of Electrical Power & Energy Systems*, vol. 23, no. 2, pp. 129–135, 2001.

[144] M. E. Baran and F. F. Wu, “Network reconfiguration in distribution systems for loss reduction and load balancing,” *IEEE Transactions on Power delivery*, vol. 4, no. 2, pp. 1401–1407, 1989.

[145] T. X. Nguyen and R. Lis, “Multiple Droop-Controlled DG Sites in an Islanded AC Microgrid for Power Losses Mitigation,” *Automatyka, Elektryka, Zak\lócenia*, vol. 14, no. 2 (52), 2023.

[146] R. Eberhart and J. Kennedy, “A new optimizer using particle swarm theory,” in *MHS’95. Proceedings of the sixth international symposium on micro machine and human science*, Ieee, 1995, pp. 39–43.

# APPENDIX

Table A. 1 Line parameters of the standard IEEE 33-node network

| From node | To node | R (Ω) | X (Ω) |
|---|---|---|---|
| 1 | 2 | 0.0922 | 0.0470 |
| 2 | 3 | 0.4930 | 0.2511 |
| 3 | 4 | 0.3660 | 0.1864 |
| 4 | 5 | 0.3811 | 0.1941 |
| 5 | 6 | 0.8190 | 0.7070 |
| 6 | 7 | 0.1872 | 0.6188 |
| 7 | 8 | 0.7114 | 0.2351 |
| 8 | 9 | 1.0300 | 0.7400 |
| 9 | 10 | 1.0440 | 0.7400 |
| 10 | 11 | 0.1966 | 0.0650 |
| 11 | 12 | 0.3744 | 0.1238 |
| 12 | 13 | 1.4680 | 1.1550 |
| 13 | 14 | 0.5416 | 0.7129 |
| 14 | 15 | 0.5910 | 0.5260 |
| 15 | 16 | 0.7463 | 0.5450 |
| 16 | 17 | 1.2890 | 1.7210 |
| 17 | 18 | 0.7320 | 0.5740 |
| 2 | 19 | 0.1640 | 0.1565 |
| 19 | 20 | 1.5042 | 1.3554 |
| 20 | 21 | 0.4095 | 0.4784 |
| 21 | 22 | 0.7089 | 0.9373 |
| 3 | 23 | 0.4512 | 0.3083 |
| 23 | 24 | 0.8980 | 0.7091 |
| 24 | 25 | 0.8960 | 0.7011 |
| 6 | 26 | 0.2030 | 0.1034 |
| 26 | 27 | 0.2842 | 0.1447 |
| 27 | 28 | 1.0590 | 0.9337 |
| 28 | 29 | 0.8042 | 0.7006 |
| 29 | 30 | 0.5075 | 0.2585 |
| 30 | 31 | 0.9744 | 0.9630 |
| 31 | 32 | 0.3105 | 0.3619 |
| 32 | 33 | 0.3410 | 0.5302 |

Table A. 2 Load parameters of the standard IEEE 33-bus network

| **Bus no.** | $V$ (kV) | Angle (rad) | $P_{Lio}$ (kW) | $Q_{Lio}$ (kvar) |
|---|---|---|---|---|
| 1 | 12.66 | 0 | 0 | 0 |
| 2 | 12.66 | 0 | 100 | 60 |
| 3 | 12.66 | 0 | 90 | 40 |
| 4 | 12.66 | 0 | 120 | 80 |
| 5 | 12.66 | 0 | 60 | 30 |
| 6 | 12.66 | 0 | 60 | 20 |
| 7 | 12.66 | 0 | 200 | 100 |
| 8 | 12.66 | 0 | 200 | 100 |
| 9 | 12.66 | 0 | 60 | 20 |
| 10 | 12.66 | 0 | 60 | 20 |
| 11 | 12.66 | 0 | 45 | 30 |
| 12 | 12.66 | 0 | 60 | 35 |
| 13 | 12.66 | 0 | 60 | 35 |
| 14 | 12.66 | 0 | 120 | 80 |
| 15 | 12.66 | 0 | 60 | 10 |
| 16 | 12.66 | 0 | 60 | 20 |
| 17 | 12.66 | 0 | 60 | 20 |
| 18 | 12.66 | 0 | 90 | 40 |
| 19 | 12.66 | 0 | 90 | 40 |
| 20 | 12.66 | 0 | 90 | 40 |
| 21 | 12.66 | 0 | 90 | 40 |
| 22 | 12.66 | 0 | 90 | 40 |
| 23 | 12.66 | 0 | 90 | 50 |
| 24 | 12.66 | 0 | 420 | 200 |
| 25 | 12.66 | 0 | 420 | 200 |
| 26 | 12.66 | 0 | 60 | 25 |
| 27 | 12.66 | 0 | 60 | 25 |
| 28 | 12.66 | 0 | 60 | 20 |
| 29 | 12.66 | 0 | 120 | 70 |
| 30 | 12.66 | 0 | 200 | 600 |
| 31 | 12.66 | 0 | 150 | 70 |
| 32 | 12.66 | 0 | 210 | 100 |
| 33 | 12.66 | 0 | 60 | 40 |

# LIST OF PUBLICATIONS

This thesis builds upon the following research publications, encompassing papers from both the Journal Publications and Monograph Publications sections.

## Journal Publications

[J1] **Tham X. Nguyen** and Robert Lis, "Optimal size and location of dispatchable distributed generators in an autonomous microgrid using Honey Badger algorithm," Archives of Electrical Engineering, pp. 871–893, 2023. (100 points-MEiN list)

[J2] **Tham X. Nguyen** and Robert Lis, "Multiple droop-controlled DG sites in an islanded AC microgrid for power losses mitigation," Automatyka, Elektryka, Zakłócenia, vol. 14, no. 2 (52), 2023. (200 points-MEiN list)

## Monograph Publications

[M1] **Tham X. Nguyen**, Optimal Capacity and Placement of Dispatchable Distributed Generations in an Autonomous Microgrid Using Differential Evolution Algorithm. Gdansk: The Gdansk University of Technology Publishing House, 2023. (80 points-MEiN list)

## Submitted Manuscripts

[S1] Muhammad Jamshed Abbass, Robert Lis, Zohaib Mushtaq, **Tham X. Nguyen**, and Muhammad Farrukh, **"**Long Short-Term Memory-based deep learning technique for predicting voltage stability in the power system," Bulletin of the Polish Academy of Sciences Technical Sciences, 2023.

[S2] Muhammad Jamshed Abbass, Robert Lis, Muhammad Awais, **Tham X. Nguyen**, and Muhammad Farrukh, **"**Convolutional Long-Short-Term Memory

(ConvLSTM)-based Deep Learning hybrid Technique for predicting Voltage Stability in a Microgrid," 2023. (prepare the manuscript to submit to peer-reviewed journal)